Design and Evaluation of an Efficient High-Precision Ocean Surface Wave Model with a Multiscale Grid System (MSG_Wav1.0)

Jiangyu Li[1], Shaoqing Zhang[*1,2], Qingxiang Liu[3], Xiaolin Yu[1,2], Zhiwei Zhang[1,2]

[1]Frontier Science Center for Deep Ocean Multispheres and Earth System (FDOMES) and Physical Oceanography Laboratory, Ocean University of China, Qingdao, 266100, China.
[2]Qingdao National Laboratory for Marine Science and Technology, Qingdao, 266100, China.
[3]College of Oceanic and Atmospheric Sciences, Ocean University of China, Qingdao, 266100, China.

Correspondence to: Shaoqing Zhang (szhang@ouc.edu.cn)

Abstract. Ocean surface waves induced by wind forcing and topographic effects are a crucial physical process at the air-sea interface, which significantly affect typhoon development, ocean mixing, etc. Higher-resolution wave modeling can simulate more accurate wave states, but requires huge computational resources, making it difficult for Earth system models to include ocean waves as a fast-response physical process. Given that high-resolution Earth system models are in demand, efficient high-precision wave simulation is necessary and urgent. Based on the wave dispersion relation, we design a new wave modeling framework using a multiscale grid system. It has the fewest number of fine grids and reasonable grid spacing in deep water areas. We compare the performance of wave simulation using different spatial propagation schemes, reveal the different reasons for wave simulation differences in the westerly zone and the active tropical cyclone region, and quantify the matching of spatial resolutions between wave models and wind forcing. A series of numerical experiments show that this new modeling framework can more precisely simulate wave states in shallow water areas without losing accuracy in the deep ocean while costing a small fraction of traditional simulations with uniform fine-gridding space. With affordable computational expenses, the new ocean surface wave modeling can be implemented into high-resolution Earth system models, which may significantly improve the simulation of the atmospheric planetary boundary layer and upper-ocean mixing.

1 Introduction

Ocean surface waves induced by wind forcing and topographic effects significantly affect the flux exchange at the air-sea interface (e.g., Garg et al., 2018; Qiao et al., 2010; Sullivan and McWilliams, 2010). Ocean surface waves can modify the underestimated intensity ~~and structure~~ of tropical cyclones in coupled models by sea surface roughness and ocean spray (e.g., Bao et al., 2000; Zhang et al., 2021). It can also mitigate the overestimated sea surface temperature in summer in ocean circulation models by enhancing ocean mixing with the help of wave breaking, wave-turbulence interaction, and Langmuir circulation (e.g., Hughes et al., 2021; Zhang et al., 2012). Besides, ocean surface waves have a contribution to the transport of sea surface floating litter (Higgins et al., 2020) and underwater spilled oil (Cao et al., 2021) because there are Stokes drifts as ocean surface waves propagate forward. Furthermore, driven by strong winds, disastrous waves with extreme wave heights (Wu et al., 2021) can cause huge economic losses and serious casualties to coastal residents (Tao et al., 2018). Therefore, obtaining the accurate distribution of wave states in time and space is extremely necessary to study atmospheric and oceanic phenomena and then guide human production and life.

Because of their small scales with wavelengths ranging from centimeters to hundreds of meters, ocean surface waves are difficult to be resolved explicitly in large-scale numerical models (Brus et al., 2021). Phase-averaged wave models widely used only describe the statistical characteristics of wave states in every fluid unit, which is dominated by source-sink terms (e.g., WAMDI group, 1988; Yang et al., 2005). Up to now, several studies have been done to enhance wave simulation accuracy, such as choosing the appropriate parameterization schemes for different external forcings (e.g., Kaiser et al., 2022; Stopa et al., 2016), optimizing the parameterizations of source-sink terms (e.g., Liu et al., 2019; Zieger et al., 2015), and implementing more physical processes (e.g., Mentaschi et al., 2015; Rogers and Holland, 2009).

A higher-resolution model consisting of finer grid units can better ~~resolve~~ describe complex topographic features and meandering shorelines (e.g., Chawla and Tolman, 2008; Tolman, 2003). Wave models with higher resolution can better express the blocking effect of small islands and take into account more local responses to high-precision environmental forcings, especially wind forcing. Thus, enhancing wave model resolution also is a very feasible way to obtain high-precision wave states. However, high-resolution simulation in the whole domain could be very expensive, which is limited by the computational resources available. It is ~~inconvenient~~ unfriendly for ~~high-precision~~ operational wave forecasting that needs to predict high-precision wave states very quickly and also blocks ocean surface waves from ~~participating~~ being incorporated into high-resolution Earth system models as a fast-response physical process at the air-sea interface (e.g., Dunne et al., 2020; Jungclaus et al., 2022). Usually, ~~one uses the coarse-resolution simulation result as an approximation if coupled systems consider ocean surface waves~~ in weather-scale numerical simulations, people use a nesting way to get local high-precision wave states and then study their effects on the air-sea interface in coupled system models. In climate-scale coupled simulations, one either does not consider the wave process (Lin et al., 2020; Ziehn et al., 2020) or simulates wave states using a coarse-resolution wave model (Bao et al., 2020; Danabasoglu et al., 2020), based on the assumption that ocean surface waves have a negligible or very small effect on the atmosphere and ocean.

Nowadays, the role of ocean surface waves in Earth system models is becoming increasingly important during this seamless climate-weather study period. ~~Due to t~~The advancement of high-performance computing (hereafter HPC) also provides us an opportunity to obtain high-precision wave states.~~,~~ Considering that high-precision operational wave forecasting and high-resolution Earth system models are in demand, ~~which~~ we need high-precision ocean surface wave modeling with high efficiency urgently. After analyzing the theory that wave modeling describes the average characteristics of wave states using the wave action density spectrum as a statistical variable, regulated by the wave dispersion relation, ~~we~~ this paper designs a new wave modeling framework based on a multiscale grid system with a variable grid resolution in geographical space. Then ~~we~~ this paper compares the performance of this system using four numerical schemes in geographical space, reveals the different reasons for wave simulation differences in two ~~areas of~~ strong wind areas, and quantifies~~y~~ the matching of ~~wave~~

~~model~~ grid resolution between wave model and wind signal. The optimized multiscale grid system is much finer in coastal areas~~,~~ but with a reasonable coarse grid spacing in open oceans. Using this grid can eliminate the disadvantages of using traditional multi-layer nesting grids. For example, ~~I~~it can eliminate the excessive usage of computational resources due to double calculations in ~~the~~ overlapping areas. It also can eliminate errors caused by the downscaling process at the boundary, which will be propagated to the inner region driven by external forcings. It still can reduce uncertainty and complexity when wave models are incorporated into a multi-layer nesting Earth system model (such as the atmosphere model WRF using a nesting and moving grid system to study typhoons).~~and the two-way information exchange, and therefore is more convenient to exchange fluxes with the atmosphere and ocean in complex Earth system models, compared with traditional multi-layer nesting.~~

This paper is organized as follows. Section 2 displays the importance and constraint of high-resolution wave simulation and analyzes the feasibility of efficient and high-precision wave modeling based on theoretical analysis of the wave dispersion relation and a series of numerical simulation experiments~~of the wave dispersion relation~~. Section 3 designs a new wave modeling framework with the unstructured triangular multiscale grid system after the comparison of different multiscale grid systems. Section 4 systematically tests and thoroughly evaluates the performance of this new modeling in deep and shallow water areas using a series of numerical experiments. Finally, section 5 gives some summary and discussions.

2 Raising the scientific idea

2.1 The importance and constraint of high-resolution wave modeling

In this section, we will first analyze the characteristics of wave simulation using traditional structured grids (or regular latitude-longitude grids) with different model resolutions by a set of experiments shown in Table 1. The design of these experiments is briefly introduced below. All physical processes in the wave model WaveWatch III version 5.16 (hereafter WW3; Tolman, 1991) are activated, of which parameterization settings can refer to Li and Zhang (2020). The needed wind forcing is from the reanalysis dataset ERA5 of the European Center for Medium-Range Weather Forecasts (hereafter ECMWF), with a spatial and temporal resolution of 0.25° and 6 hours, respectively. The shoreline data can be obtained from the Global Self-consistent Hierarchical High-resolution Shoreline (hereafter GSHHS) dataset, National Oceanic and Atmospheric Administration (hereafter NOAA). The topography data is from the NOAA ETOPO1 dataset with a spatial resolution of 1′. For simplicity, we choose the Asia-Pacific area (39°E-178.5°E, 16°S-62.5°N) to explain our scientific idea. The required wave boundary information is from the global wave simulation (0°-359°, 75°S-75°N) using a traditional structured grid with 1° resolution driven by ERA5 wind.

Driven by the same ERA5 wind, Figure 1 shows the spatial distributions of significant wave heights (hereafter SWHs) around Taiwan Island, China (119°E-123°E, 21°N-26°N) in January 2018. They are from wave simulations (briefly as "WS") using a traditional structured grid system (briefly as "s" in the superscript) with 1°, 0.5°, 0.25°, and 0.125° model resolutions (denoted as the subscript), called WS_1^s, $WS_{0.5}^s$, $WS_{0.25}^s$, and $WS_{0.125}^s$ in Tab. 1. The ability to identify land and ocean in wave models is a prerequisite to obtain accurate wave states. However, there is an obvious mismatch between the real (surrounded by black lines, from the GSHHS dataset) and identified (white fill) locations of Taiwan Island and the Chinese mainland, particularly in WS_1^s and $WS_{0.5}^s$ (Figs. 1a and 1b). Moreover, ~~T~~the lack of representation of some islands is a major local error source (Tolman, 2003). When model resolutions are coarse (Figs. 1a and 1b), the blocking effects of the Penghu Islands (for example) are not well-expressed. Unsurprisingly, as model resolutions increase in $WS_{0.25}^s$ and $WS_{0.125}^s$ (Figs. 1c and 1d), the above poor shoreline fitting and island representativeness are improved. Nevertheless, even if the model resolution is increased to 0.125 ° in Fig. 1d, there is still a gap between the real and identified shorelines and topography. For instance, Green Island is too small to be resolved in wave models, which will be approximated with obstruction grids (Chawla and Tolman, 2008) (used in this paper) or parameterized with a source term (Mentaschi et al., 2015) instead.

It is generally believed that the finer the model resolution is, the more accurate wave states can be obtained. Since we don't have real wave states in the whole domain, simulation results obtained from the experiment using the structured grid with 0.0625 ° resolutions (named $WS_{0.0625}^s$ in Tab. 1) are considered as a reference to verify the influence of different model resolutions on wave simulation accuracy. The linear interpolation method is used to calculate the SWH root mean square differences (hereafter RMSDs). Figure 2 shows the spatial distributions of SWH RMSDs around the Asia-Pacific area in January 2018. The simulated RMSDs are smaller as the model resolution gets finer. When the model resolution is 1 °, 0.5 °, 0.25 °, and 0.125 ° (Figs. 2a-2d), the corresponding RMSD is 0.11, 0.07, 0.04, and 0.02 m, respectively.

Figure 3 shows the time consumption of the above simulation experiments using a structured grid system under the same computational condition. When the model resolution is coarse (WS_1^s, $WS_{0.5}^s$, $WS_{0.25}^s$, and $WS_{0.125}^s$), it takes very little computational time and we can afford it easily ~~the consumed time is acceptable for us~~. However, when the model resolution is improved from 0.125 ° to 0.0625 °, the consumed time increases from 1.92 to 33.79 hours dramatically. The more likely reason for this phenomenon, in addition to usual reasons (an increased model resolution and a large amount of model data output), ~~most likely due to the WW3~~ is the parallelism called card deck used in WW3 ~~and a large amount of model data output~~. In this mechanism, one computing core calculates the wave state of one water point (not all water points in a small domain), and the wave states of two adjacent water points are calculated by different cores. Please see Abdolali et al. (2020) for a more intuitive understanding. The common approach to shortening computational time is to add parallel computing cores if computational resources are abundant. It is feasible when the cores used are smaller than a certain threshold. ~~While a~~As the number of cores increases, the saved computational time can be offset by the increased time from the excessive information exchange between the cores (Feng et al., 2016). This offset situation is more obvious when you use a parallel scheme like the card deck. Not to mention, when computational resources are limited, it is impossible to achieve high-resolution wave simulation. In the future, if higher-resolution, longer-duration, and larger-area wave states are needed, it will take huge computational resources and time, even as expensive as the atmosphere-ocean coupled models (Brus et al., 2021). This is the situation we don't want to happen, and it needs to be solved urgently.

In summary, higher-resolution wave models have better ability in shoreline fitting and topography description (Fig. 1) and can simulate more precise wave states (Fig. 2). However, high-resolution wave simulation with a uniform fine-gridding space requires huge computational resources (Fig. 3), which is a big challenge to high-precision operational forecasting systems and high-resolution Earth system models. Therefore, efficient and high-precision wave modeling is very necessary and urgent.

2.2 Analysis and understanding of the wave dispersion relation

As we know, wave modeling is regulated by the wave dispersion relation, here we will reintroduce it. The dispersion relation, a relationship between relative frequency (σ), wave number (k), and water depth (d), represents the nature and characteristics of ocean surface waves. It is expressed by $\sigma^2 = gktanh(kd)$, where g and $tanh$ are the gravitational acceleration and hyperbolic tangent function, respectively. In classical ocean surface wave theory, the magnitude relationship of $\frac{d}{l} > \frac{1}{2}$, $\frac{1}{20} < \frac{d}{l} \leq \frac{1}{2}$, and $\frac{d}{l} \leq \frac{1}{20}$ is used to determine deep, intermediate, and shallow water areas, where l represents the wavelength. After a simple mathematical limit operation, the wave dispersion relation $\sigma^2 = gktanh(kd)$ is simplified to $\sigma^2 = gdk^2$ and $\sigma^2 = gk$ in shallow ($\frac{d}{l} \leq \frac{1}{20}$) and deep ($\frac{d}{l} > \frac{1}{2}$) water areas, respectively.

To more vividly show the meaning of the wave dispersion relation, a schematic diagram of wave propagation characteristics described in different water areas and simulated with different spatial resolutions is shown in Figure 4. In deep water areas, ocean surface waves have large wavelengths and long wave periods. Because they are insensitive to topographic features (represented by water depth d in the above dispersion relation), wave models with coarse or fine resolution, consisting of coarse or fine grid units, have good performance in simulating wave states almost without losing accurate responses to wind signals. When ocean surface waves travel from deep to intermediate water areas (their boundary is marked with a green vertical bar), the wavelength decreases, and the wave height increases. The effects of topographic features (thick black line) on the wave states are activated. These features (such as sea peaks and valleys) are well-represented/excessively-smoothed using fine/coarse resolution models (thick red/blue lines), which directly affects wave simulation accuracy. Moreover, when ocean surface waves reach coastal areas with very shallow water, more complex physical processes should be considered, such as depth-induced wave breaking, wave scattering and reflection, and so on. However, the described topographic features are distorted even when using fine-resolution models, let alone coarse-resolution models. This situation will directly leads to very poor simulation precision (as shown in Fig. 1d). Thus, wave model resolution needs to be improved constantly, especially in coastal areas. It's worth mentioning that this figure is a schematic diagram and does not represent the actual wave modeling process (using wave action density spectrum as the integral variable) and spatial scales of ocean surface waves, only to illustrate our idea.

Next, we will use numerical simulation results to further understand the above theoretical characteristics. The wave simulation using a structured grid with 0.0625° resolutions is regarded as the reference experiment, and that with 1°, 0.5°, 0.25°, and 0.125° resolutions separately is regarded as a control experiment (four control experiments are here). Figure 5 shows the evolution of SWH differences (control minus reference, representing errors) around the South China Sea (105°E-125°E, 0°N-27°N) on the first day of model integration. The wave states are resting at the first moment of the model run

(00:00 UTC, November 1, 2017). After that, ocean surface waves begin to generate and propagate, induced by wind forcing and topographic effects. Driven by strong wind (magenta arrows in the first column of Fig. 5), ocean waves in the northwest South China Sea have rapid responses at the 1st integral time step (00:15 UTC, November 1, 2017). Because coarse-resolution models lack representation of complex topography (WS_1^s for example), SWH differences are generated at the beginning of the model run~~, especially in the central part of the South China Sea where the water depth gradient is very large (northeastern-southwestern direction)~~. They are propagated forward driven by wind~~ along the wave motion way~~, which can be observed clearly at the 4th integral time step in Fig. 5a. As time passes, the simulated differences are constantly generated and propagated to the deep ocean, driven by the strong wind (Figs. 5e and 5i). At the 24th hour of model integration, they are almost distributed over the whole South China Sea (Fig. 5m). At the same time, driven by weak wind, SWH differences are small and their effects on the surrounding sea areas are weak relatively in the southeast South China Sea (the first column of Fig. 5). As we expected, with the increase of model resolution, there is a higher representation of topographic features and a more accurate response to local wind, so the simulated differences gradually decrease. They are almost imperceptible when the model resolution is 0.125 °($WS_{0.125}^s$, the fourth column). Please see Zhongsha Islands circled by dashed boxes in the first column and last row for a more intuitive observation.

2.3 On the feasibility of efficiently modeling ocean surface waves

Based on the above theoretical analysis and numerical simulation, we have the following understanding. (1) In shallow and intermediate water areas, wave states are very sensitive to topographic features, especially in coastal areas. Therefore, a finer-resolution wave model consisting of smaller fluid units is necessary to better describe the complex topographic features and meandering shorelines. This way can reduce wave simulation errors in shallow water areas and weaken their effects on the surrounding sea areas. It also takes into account more local responses driven by high-precision environmental forcings, especially wind forcing. (2) In deep water areas, wave states are insensitive to topographic effects. Then, a coarse-resolution model is suggested to save computational resources without sacrificing accurate responses to external forcings.

Therefore, similar to the classical wave theory, we choose the magnitude relationship between $\frac{d}{l}$ and $\frac{1}{2}$ to determine shallow ($\frac{d}{l} \leq \frac{1}{2}$) and deep ($\frac{d}{l} > \frac{1}{2}$) water areas for simplification. Here, the "shallow" water areas are a general notion, including the shallow and intermediate water areas defined in classical theory, where topographic effects should be taken into account in wave simulation. It's important to note that we only follow the idea of dividing different water areas from the classical theory, and do not change the expression of the wave dispersion relation in all numerical simulation experiments. Previous studies have used a specific/gravity water depth as a criterion to classify different waters (e.g., Brus et al. 2021; Li, 2012; Mao et al., 2015), which has achieved good results in saving wave simulation time. The method used in this paper is a direct application of the wave dispersion relation, then can minimize the number of fine grids. This will further improve wave simulation efficiency, which is very much needed for the Earth system models considering the ocean surface wave process.

Therefore, we can design a new wave modeling framework with a multiscale grid system much finer in coastal areas but relatively coarse in open oceans, to achieve efficient and high-precision wave simulation. This wave modeling idea is feasible preliminarily since the global ocean is almost covered by deep water with only a small portion of shallow water, such as only 2.7% of shallow water in the Asia-Pacific area. Next, we will introduce the different implementations of building this framework, the factors to consider for designing a multiscale grid system, and the performance of this framework in detail.

3 Design of an efficient and high-precision wave modeling framework

3.1 Multiscale grid systems

Multiscale grid systems are usually made up of multiple polygons with different spatial sizes. Now, two multiscale grid systems are available in wave models. One is made up of rectangles with different sizes (Li, 2011), named unstructured rectangular multiscale grid in this paper. ~~And t~~The other is made up of triangles (e.g., Roland et al., 2009; Zijlema, 2010), called unstructured triangular multiscale grids (“utms” for short, superscripts of experiment names in Tab. 1). They have similar design ideas, setting fine-resolution meshes in shallow water areas to enhance simulation accuracy, and coarse-resolution meshes in deep water areas to save computation resources. At the same time, to avoid a sharp ~~change~~ gradient of ~~in~~ coastal water depth, setting modest-resolution meshes in transitional water areas ensures a stable calculation. Note that the transitional water areas here are ~~a~~ part of deep water areas, which are different from the intermediate water areas in the classical wave theory. Now, using simple diagrams in Figure 6, the generation steps of these two grids both with variable resolutions from Δx in shallow water areas to 2Δx in transitional water areas and then to 4Δx in deep water areas, and their performance are briefly introduced. Note that curvilinear grids as an extension of traditional structured grids (Rogers and Campbell, 2009) are not discussed here.

3.1.1 Generation of multiscale grid systems

Steps for making unstructured rectangular multiscale grid systems are described as follows (Hou et al., 2022). The study area can be divided into 2×2 rectangular groups with 4Δx resolutions. Looping for every group, if there is no land inside, the group is marked with blue lines in Fig. 6a. Otherwise, the group can be further divided into 2×2 boxes with 2Δx resolutions. Similarly, looping for every box, it is marked with magenta lines if the box is covered with water everywhere. Or, the box is divided into 2×2 cells with Δx resolution. Cells near shorelines can be identified as land or ocean by judging the land-ocean ratio in every cell. The actual and fitted shorelines are marked with thick black and red lines, respectively. Now, the unstructured rectangular multiscale grid is generated. Note that the scale of two adjacent meshes is 1:1 or 1:2.

The steps of generating an unstructured triangular multiscale grid are described in the following. In the beginning, obtaining fine shoreline data is necessary. Next, with the help of shorelines and two types of control lines marked with thick red, magenta, and blue lines in Fig. 6b, the spatial resolution in shallow, transitional, and deep water areas can be set to Δx, 2Δx, and 4Δx, respectively. Once reasonable control lines are ready, a lot of triangles with different spatial sizes are generated quickly. Now, making the unstructured triangular multiscale grid is finished. Note that if the grid resolution is set to 4Δx, this does not mean that the length of three elements in every triangle is 4Δx exactly, but varies within a reasonable range around 4Δx (±20% used in this paper).

3.1.2 Comparison of two grid systems

Here will further compare the performance of wave simulation using different grid systems with the same fine resolution. The lower panels of Fig. 6 show spatial distributions of SWHs from wave simulation using the traditional structured and unstructured triangular grids both with 0.125°resolutions (named $WS_{0.125}^{s}$ and $WS_{0.125}^{ut}$ in Tab. 1. Here show wave states in a small area of the Asia-Pacific region for clarity). It's like using the finest spatial resolution (Δx) throughout the whole domain in the upper panels (Figs. 6a and 6b). Compared to those using the structured grid (red lines in Fig. 6c), wave models using the unstructured grid (red lines in Fig. 6d) have a better ability to fit the actual land-ocean shorelines (black lines in Figs. 6c and 6d). This is the reason why the latter has simulation results at all 9 available Chinese oceanic stations that are very close to shorelines (Table 2), while the former has simulation data only at 4 stations, including XCS, NJI, BSG, and DCN, respectively. Since wave simulation using different grids performs similarly at these four stations, the results at station BSG are used here as an example to illustrate. This station is marked with yellow stars in Figs. 6c and 6d ~~lies~~ near a group of small islands (a distance from the mainland), which are not enough to be resolved in wave models using structured or unstructured grids with 0.125° resolutions. The former uses sub-grid obstacles with different levels of transparency for approximation, while the latter directly treats them as water areas. When waves travel from the open ocean to the mainland in a southeast direction, ocean surface waves at this observation station behind these islands are underestimated resulting from a lot of wave energy dissipation caused by excessive blocking in wave models using a structured grid. For example, the observed average SWH is 1.28 m at the valid observed time in July 2018, and the simulated SWHs are 1 m and 1.23 m in $WS_{0.125}^{s}$ and $WS_{0.125}^{ut}$ (Figs. 6c and 6d), respectively. Therefore, wave models using the unstructured triangular grid have more advantages than those using the traditional structured grid in shoreline fitting and coastal simulation accuracy, while they take almost the same computational time (2.04 and 1.92 hours in the following Figure 13).

3.2 Design of a new wave modeling framework

Considering the advantages of triangular grids in coastal areas (e.g., Engwirda, 2017; Roberts et al., 2019) and the follow-up sustainability of this work, we design the first version of a new wave modeling framework using an unstructured triangular multiscale grid to achieve the goal of efficient and high-precision wave simulation. The generated steps in Surface-water Modeling System software (SMS) are described as follows. Similar to previous papers, we first~~will~~ empirically set the spatial resolution of this multiscale grid in different water areas. In the ~~following~~ next section, we will optimize this grid after evaluating its performance through a series of experiments. ~~show the performance of this grid setting and optimize it further, along with~~ Finally, we will give some tips for designing the grid resolution, particularly in deep water areas, which is friendly for readers to follow.

Step 1: obtaining and optimizing shorelines. Theoretically, with the support of high-resolution topography and shoreline datasets, mesh resolution can be refined infinitely (e.g., Li and Saulter, 2014) in shallow water areas to simulate higher-precision wave states. Fine shoreline data comes from the NOAA GSHHS dataset with a 1 km resolution, and topography data comes from the NOAA ETOPO1 dataset with a 1′ resolution. In practice, trading off the simulation accuracy and computational resource consumption, we set shoreline resolution to 0.125° (red lines in Figure 7) for a preliminary test. Proper shoreline adjustment is suggested if there is any unsuitability, which is very important to accurately obtain coastal wave states (Fig. 6d). When finer shoreline data is available in key areas, the shorelines should be further refined if necessary.

Step 2: setting control lines with different spatial resolutions. As stated in section 2.2, wave states are insensitive to topographic features in deep water areas, which can be simulated using coarse-resolution models. Here, we determine the boundary locations between shallow and deep water areas (their definitions differ from the classical definitions and are introduced in Section 2.3 above) based on the relationship between the water depth and half of the minimum mean wavelength. These two variables are derived from wave simulation results with a resolution of 0.0625° ($WS_{0.0625}^{s}$ in Tab. 1) in 2018. Then, the control lines following this boundary can be set to 0.5° (magenta lines in Fig. 7). To further shorten the computational time, we set other control lines with 1° resolution (blue lines in Fig. 7) in the deeper ocean, where the global grid resolution is suggested in Tolman (2003). Note that the spatial locations of these two types of control lines are adjusted by constant testing to achieve a stable calculation and maximum benefit.

Step 3: generating the unstructured triangular multiscale grid. Once reasonable control lines and open boundaries (green lines in Fig. 7) are determined, a lot of triangles with different spatial sizes are quickly generated in SMS ~~software~~. This software has a powerful function to identify poor-quality meshes (just a tiny fraction of total meshes), such as one node connecting too many elements (8 used in this paper), or a triangle with too big (130 degrees used in this paper), or too small (30 degrees used in this paper) interior angles. It is recommended to adjust these poor-quality meshes ~~Some adjustments to the poor mesh quality are suggested~~ to ensure stable computation, which takes very little time.

Now, the first version of the wave modeling framework using the unstructured triangular multiscale grid with the spatial resolution of 0.125°, 0.5°, and 1° in shallow, transitional, and deep water areas is finished (WS_{multi3}^{utms} in Tab. 1). Fig. 7 shows that the spatial size of these meshes gradually and smoothly increases from coastal areas to deep oceans with the help of control lines. ~~Currently, a tool named OceanMesh2D (Roberts et al., 2019) including a set of MATLAB functions is more flexible and automated in making unstructured triangular multiscale grid systems. Then in the future, the grid optimization in the coastal area and the expansion of the regional grid to a global grid are very convenient and do not take much time.~~

4 Evaluation of wave simulations

4.1 Evaluation with different propagation schemes

Wave models describe the evolution of wave action density spectrum in the geographic space (including longitude and latitude) and spectral space (including frequency and direction), dominated by source-sink terms. Since we only change the grid size in geographic space, here we will evaluate the performance of wave simulation using the unstructured triangular multiscale grid (WS_{multi3}^{utms} in Tab. 1) in this space. There are four propagation schemes available in wave model WW3, including CRD-N, CRD-FCT, CRD-PSI, and implicit N. Please see Roland (2009) for more detailed descriptions. After 14-month numerical integration (from November 1, 2017, to December 31, 2018, UTC) using four numerical schemes separately, WS_{multi3}^{utms} can run stably. This indicates that it is feasible that wave energy can propagate smoothly and continuously on multiple meshes with different spatial resolutions. Wave ~~S~~simulation results using four spatial propagation schemes and their comparison are shown in Figure 8 and their spent computation time ~~spent~~ is listed in Table 3.

Fig. 8a displays SWH distributions of wave simulation using the propagation scheme CRD-N (the default scheme, first-order ~~accuracy~~ precision in time and space) in January 2018 (the month with the largest differences when wave simulation uses four numerical schemes in 2018). There is a high correlation between the magnitude of wave height (color shaded) and wind intensity (magenta arrows), for example, in the northern Pacific Ocean (the northern Indian Ocean and equatorial Pacific region), ocean surface waves have large (small) wave heights driven by strong (weak) wind. Figs. 8b-8d show the SWH differences between wave simulation using CRD-PSI, CRD-FCT, and implicit N schemes and that using the CRD-N scheme (Fig. 8a), respectively. The differences between wave simulation using nonlinear CRD-PSI and linear CRD-N schemes are relatively small (Fig. 8b) and the spent calculation time ~~spent~~ of these two experiments is roughly the same (Tab. 3). Roland (2009) ~~said~~ mentioned that the CRD-PSI scheme is second order only in cross flow direction and is first order in longitudinal flow direction and time. There are obvious simulation differences in Fig. 8c and they propagate forward driven by wind (wind vectors shown in Fig. 8a).~~, especially in the complex topographic areas,~~ This is because CRD-FCT has second-order ~~accuracy~~ precision in time and space, and then wave simulation using it is easier to produce differences in complex topographic areas (especially in the archipelago region of the eastern equatorial Pacific ocean) compared with that using the linear CRD-N scheme. Also using this CRD-FCT scheme ~~which also~~ leads to ~~its~~ the lowest calculation efficiency among the four schemes (Tab. 3). There are only slight differences in Fig. 8d because CRD-N and implicit N schemes both use a linear scheme. Although there are differences in wave simulation results using four schemes, these differences are almost within a scale of ±0.1m, which is negligible. ~~they can be negligible~~ Similar performance is given after verifying with observations at 9 available Chinese oceanic stations (Tab. 2) (not shown). The wave parameters of the mean wave period (hereafter MWP) and mean wave direction (hereafter MWD) also have negligible simulation differences~~similar spatial distributions~~ (not shown). On the whole, wave simulation with the explicit and implicit schemes has similar simulation accuracy for Courant-Fredrichs-Levey (CFL) <1 (WW3DG, 2019). It should be noted that when wave simulation uses multiscale grid systems, it is better to extend the computing area outward by 3° (1° spatial resolution at most boundary areas) to reduce the influence of open boundaries on the concerned area, especially if the wave model uses the CRD-FCT scheme that has a two-order precision.

Wave simulation results using the unstructured triangular grid with 0.125 ° resolutions in the whole domain ($WS_{0.125}^{ut}$ in Tab. 1) are regarded as a reference to evaluate the performance of WS_{multi3}^{utms}. ~~, whose~~The comparison is listed in Tab. 3. Compared with $WS_{0.125}^{ut}$ using four schemes respectively, simulation results of WS_{multi3}^{utms} using the corresponding~~four~~ scheme~~s~~ are ~~basically~~ almost the same. Wave parameters of SWH and MWP both have very small simulation differences (about 0.1m and 0.2s, respectively) and large correlation coefficients (hereafter CCs, about 0.98). The performance of MWD is slightly worse (about 24 ° simulation differences and 0.92 CCs) than SWH and MWP, and this similar situation also can be seen in Pallares et al. (2017) ~~but is acceptable~~. As we expected, wave simulation using a multiscale grid system has a high computational efficiency, saving more than 80% of computational time. This is consistent with the theoretical analysis in section 2.2. Considering the simulation accuracy and computational efficiency (Tab. 3), the default scheme CRD-N will be adopted in the following study.

~~The first three numerical schemes (including CRD-N, CRD-PSI, and CRD-FCT) are explicit schemes that are restrained by the CFL condition, which limits the nearshore resolution to 200 m in operational systems considering calculational costs. The fourth scheme is an implicit scheme, refining coastal areas down to 10-50 m without CFL constraint. Although the implicit N scheme takes much computational time, it could be a good choice for accurate coastal wave simulation with the help of a new parallelization algorithm, domain decomposition (Abdolali et al. 2020). In the future, we can reasonably set the integral time step in the case of CFL>1, to further reduce calculation time costs. In this paper, since the current coastal resolution has not reached the order of 100 meters, the default scheme CRD-N will be adopted in the following study.~~

4.2 Evaluation of the influences of strong wind

The atmospheric wind is an important energy source for ocean surface waves (e.g., Roland and Ardhuin, 2014), then its seasonal characteristics will affect the evolution of wave states. Here we use the reference and control experiments to evaluate the influences of strong wind. The former uses unstructured triangular grid with 0.125 ° resolutions in the whole domain (named $WS_{0.125}^{ut}$ in Tab. 1), and the latter uses unstructured triangular multiscale grid with a varying resolution (0.125 °, 0.5 °, and 1 °) in study areas (named WS_{multi3}^{utms} in Tab. 1). These two experiments share the same shorelines and grid resolution in shallow water areas, but the control experiment has a coarser grid resolution in deep water areas. In this section, two experiments are driven by the same ECMWF ERA5 wind, and ~~Figure 9 shows~~ the spatial distributions of SWH RMSDs in four seasons are shown in Figure 9. Compared to the reference $WS_{0.125}^{ut}$, simulation differences of WS_{multi3}^{utms} are very small in most ocean areas (less than 0.1 m) (left panels), such as south of the equator~~ial~~ region and northern Indian Ocean region. However, in the north of the northern Pacific Ocean, there are obvious differences in all seasons, especially in boreal winter (more than 0.15 m) shown in Fig. 9a. Similar visible differences also can be found in the west of the northern Pacific Ocean in the autumn (Figs. 9g and 9h). Wind distributions in this area (~~not shown~~magenta arrows in left panels of Fig. 9) show that

~~the equatorial region has very weak wind and the northern Indian Ocean is affected by monsoon but with moderate wind intensity. T~~the north and west of the northern Pacific Ocean are affected by strong wind, that is westerly wind and tropical cyclones, respectively. We know that when the spatial resolution of wind forcing and wave models is inconsistent, wind signals will be interpolated onto the wave model grid before model integration. Chen et al. (2018) tested the effect of a smoothed wind on wave simulation in an ideal experiment, and the results showed that it reduced the wave energy magnitude. ~~compared the effect of coarse-grid wind forcing interpolating to fine-grid wave models on the wave energy. In this paper~~Then, we propose a hypothesis that if the wind is very strong and the wind direction changes rapidly, wind signals will be over-smoothed during the interpolation process (wind forcing with 0.25° resolutions and wave models with 1° resolution), resulting in poor wave simulation accuracy.

To confirm this hypothesis, we encrypt the unstructured triangular multiscale grid in the north of the northern Pacific Ocean for a preliminary test. As shown in Fig. 7, keeping other areas unchanged, we divide the northern Pacific Ocean areas filled with grey (surrounded by a blue solid line) into two small areas named Area1 and Area2, delineated with a cyan dashed line (located at 27°N). Only the mesh resolution in Area1 is changed from 1° to 0.5°, and the mesh setting in Area2 remains the same as before. Now, the optimized unstructured triangular multiscale grid is generated. Using this grid, a similar numerical simulation (named $WS_{multi3(new)}^{utms}$ in Tab. 1) is done. We can see that its simulation differences in the northern Pacific Ocean are largely mitigated (less than 0.1 m) (right panels of Fig. 9) compared with WS_{multi3}^{utms} (left panels of Fig. 9). ~~, while two experiments contain almost the same grid numbers (Tab. 1) and take almost the same computational time (in the following Fig. 13).~~ While there are still some visible differences in the boreal winter (Fig. 9b). We know compared with other seasons, the wind in this season is stronger and changes faster. This situation will lead to over-smoothing wind energy when the wind forcing is interpolated onto wave models' grid and a larger splitting error when wave model WW3 uses an explicit scheme (CRD-N used here) (Roland, 2009). Splitting errors occur ~~This is~~ because of a fluctuation splitting scheme used for the integration of geographical, spectral advection terms and source terms ~~is operated by using a fluctuation splitting scheme if wave model WW3 with the explicit scheme (here uses CRD-N). This will introduce splitting errors, especially when wind varies strongly in geographical space (Roland, 2009).~~ Chen et al. (2018) mitigated the splitting error by using small time steps, but with little effect. If using the implicit N scheme, WW3 integrates the wave action equation directly without splitting error (Abdolali et al. 2020; Sikiric et al. 2018), then it will have slightly smaller simulation differences than that using the explicit CRD-N scheme. ~~then these differences are almost invisible at the current colorbar scale (not shown). Chen et al. (2018) mitigated the splitting error by using small time steps, but with little effect.~~ Simulation differences of MWD and MWP are also alleviated. As their differences are small, the improvement is not as obvious as the SWH (not shown). In terms of computational efficiency, $WS_{multi3(new)}^{utms}$ has only a slightly larger number of grids than WS_{multi3}^{utms} (Tab. 1), these two experiments take almost the same computational time (in the following Fig. 13).

Different tropical cyclones vary greatly in time, space, and intensity, which will have important effects on wave simulation accuracy. As shown in Figs. 9f and 9h, locations of large simulation differences overlap partial tracks of some typhoons (magenta lines). The simulated SWH differences ~~from wind sea and swell~~ both have a high correlation with wind intensity in active typhoon areas. The large differences often occur when the wind speed exceeds 50 m/s. ~~As shown in Figs. 9e and 9g, the simulation difference locations overlap typhoon tracks (magenta lines) partially.~~ Xu et al. (2017) stated that if the wind signal is not enriched from coarse grid to fine grid, only encrypting wave model resolution has little effect on wave simulation accuracy. Now, the wind forcing we used is from the reanalysis dataset ECMWF ERA5 with a coarse spatial resolution (0.25 °lat*0.25 °lon). It is unable to reproduce the typhoon process well, resulting in underestimated wave simulation results (as shown in the following Figures 11b and 11d) (Hsiao et al., 2020; Jiang et al., 2022; Wu et al., 2020). ~~Considering that typhoons cannot be accurately reproduced in the current coarse-resolution reanalysis atmosphere dataset ERA5 (0.25 ° resolutions, as shown in the following Figure 11b) (Hsiao et al., 2020),~~ Then we preliminarily suggest that the grid resolution in whole active typhoon areas consistents with the spatial resolution of wind forcing to avoid missing wind signals. In the next paper, we will revise this long-duration reanalysis dataset using typhoon parameters to get a more accurate wave state, analyze the relationship between large simulation differences and typhoon intensity, and then determine the specific area of multiscale grid encryption to further improve simulation efficiency.

In a word, in deep water areas, wave simulation using coarse-resolution grids can achieve the goal of enhancing computational efficiency without sacrificing simulation accuracy. According to the wind intensity, some suggestions are given for designing unstructured multiscale grid systems in these areas. (1) In active typhoon areas, we suggest preliminarily the spatial resolution of multiscale grid systems to be consistent with that of wind forcing to accurately capture the rapidly changing wind characteristics. (2) In the westerly zone, such as 30 °N-60 °N areas, the spatial resolution of multiscale grid systems ~~should~~ could be twice coarser than that of wind forcing to avoid over-smoothing wind signals. (3) In moderate or weak wind areas, the grid resolution of wave models could be 4 times coarser than that of wind forcing to shorten the computational time consumption.

4.3 Evaluation of influences of complex topography

With the advancement of HPC, ultra-high-~~-~~ resolution ~~Earth system~~ coupled models have been widely developed to understand air-sea interactions. For example, Li et al. (2020) have developed three versions of coupled models in the Asia-Pacific area, of which the highest-resolution version is a 3 km atmosphere coupled with a 3 km ocean. This coupled system doesn't currently achieve online wave coupling because a high-resolution wave simulation has low computational efficiency, as we described earlier (Fig. 3). In this section, we will focus on evaluating the effect of increasing spatial resolution in coastal areas on wave simulation accuracy and computational efficiency, and explore the possibility of using a multiscale grid to achieve efficient and ultra-high precision wave simulation. Considering that ~~However,~~ the highest ~~-~~resolution ~~spatial resolution~~ of the ~~above designed~~ unstructured triangular multiscale grid ($WS_{multi3(\mathrm{new})}^{utms}$) designed above in these areas is 0.125 ° (about 13 km), ~~which is still hard to describe actual shorelines and complex topographic effects in coastal water areas. Here, supported by the fine dataset,~~ we will encrypt~~increase~~ the grid resolution in coastal areas around the South China Sea (circled by a cyan solid box in Fig. 7) for further testing. The steps are as follows: (1) designing the shorelines with 0.0625 °

resolutions (about 7 km); (2) adjusting new control lines with 0.125 ° resolutions in suitable locations; (3) generating the new meshes in shallow water areas; and (4) replacing these meshes in the ~~first~~ previous version ($WS_{multi3(new)}^{utms}$)~~.~~. Now, a finer unstructured triangular multiscale grid is finished (not shown). Then, a similar numerical experiment using it is done, named WS_{multi4}^{utms} in Tab. 1.

Similar to the last section, we still design the reference experiment using a structured grid with 0.0625 ° resolutions in the whole domain (named $WS_{0.0625}^{s}$ in Tab. 1), to evaluate the performance of this control experiment (WS_{multi4}^{utms}). Since the meshes are modified only in shallow water areas, we use observation data from three Chinese oceanic stations named BSG (marked with yellow stars in Figs. 6 and 7), DSN, and ZLG (marked with yellow stars in Fig. 7) to evaluate ~~the above~~ simulation results of the control and ~~the~~ reference ~~with a structured grid, named $WS_{0.0625}^{s}$ in Tab. 1~~. Figure 10 shows the scatter diagram of the observed and simulated SWHs at the BSG station within ~~at~~ the valid observed time in four seasons of 2018. As described in section 3.1.2, wave simulation using a structured grid over-blocks wave energy at station BSG, resulting in the SWH underestimation. This situation is still not alleviated when the spatial resolution is increased from 0.125 ° (Fig. 6c) to 0.0625 ° (Figs. 10a, 10c, 10e, 10g). The WS_{multi4}^{utms} without considering the island's blocking effect has a good performance (Figs. 10b, 10d, 10f, 10h). The SWH root mean square errors (RMSEs) are reduced by about 35% in every season. ~~In terms of computational efficiency, WS_{multi4}^{utms} (0.63 hours in Fig. 13) takes much less computational time than $WS_{0.0625}^{s}$ (33.79 hours in Fig. 3).~~

We further analyze the temporal evolution of observed and simulated wind speeds and SWHs at the BSG station in February and July 2018 (an example of boreal winter and summer), respectively. ~~Fig. 11 shows a good agreement between~~ As we expected, the observed wind intensity and SWH magnitude have a good agreement ~~from the observation~~, both plotted with black lines in Fig. 11. When the wind is strong, the SWH is large, more obviously in July (Figs. 11b and 11d). Fig. 11 also shows the simulated SWHs driven by the same reanalysis wind, plotted with colored lines. It is noted that the ECMWF ERA5 dataset has no reanalysis data available at this station because its spatial resolution is too coarse to identify this station~~no observed wave data is available at this station because the spatial resolution of the ERA5 dataset is too coarse~~. Simulation results using the multiscale grid (red lines) and structured grid (blue lines) have a similar evolution but the former is closer to the observation (black lines), whether under low-moderate wind speeds (Fig. 11c) or high wind speeds as the typhoon passes through (typhoon Maria in Fig. 11d). In terms of computational efficiency, WS_{multi4}^{utms} (0.63 hours in Fig. 13) takes much less computational time than $WS_{0.0625}^{s}$ (33.79 hours in Fig. 3). Therefore, in shallow water areas (with a water depth greater than 10 meters), wave simulation using the unstructured multiscale grid can improve the description of complex shorelines and topography and enhance wave simulation precision. Similar to the BSG station, the performance of the control and reference experiments at DSN and ZLG stations are also evaluated. However, because the water depth at these two stations is too shallow (less than 10 meters, in Tab. 2), wave model WW3 using these two grids has similar underestimated behavior (not shown). This underestimation also occurs even though the wind magnitude and evolution from ECMWF ERA5 are similar to those from observation (although under this circumstance, the wave simulation using a multiscale grid is closer to observation than that using a structured grid) (Fig. 11a and 11c). This indicates that it is urgent to enhance the simulated ability of wave models in shallow water areas. ~~Furthermore, we see that wave simulation results are underestimated (e.g., Wu et al., 2020), especially in the passing of tropical cyclones (e.g., Chen et al., 2018; Jiang et al., 2022). This indicates that the wind intensity from the ERA5 dataset needs to be corrected to obtain accurate wave states when typhoons occur. At the same time, we also learn that wave model WW3 using these two grids at other oceanic stations (DSN and ZLG, in Fig. 7) have similar underestimated behavior since the water depth at both stations is less than 10 m. Then it is urgent to enhance the simulated ability of wave models in coastal areas.~~

4.4 Evaluation of the applicability

Through the systematic tests above, we know that the WW3 wave model with a multiscale grid system is feasible and has a good performance in simulation accuracy and computational efficiency. Here, we will continue to test its applicability based on the previous section. Since there are a few ~~triangles~~ meshes with 0.0625 °resolutions in WS^{utms}_{multi4}, we still use $WS^{ut}_{0.125}$ as the reference to evaluate the performance of this control experiment (WS^{utms}_{multi4})~~for evaluation~~. Figure 12 shows that the two simulation results have negligible differences in 2018. In detail, the RMSDs of SWHs, MWPs, and MWDs are all less than 0.1 meters, 0.23 seconds, and 32 degrees in Table 4, respectively. The CCs of SWHs and MWPs are around 0.99, and the MWD CCs are around 0.95. There is a slight~~ but acceptable~~ impact on MWD. A similar phenomenon can also be seen in Pallares et al. (2017), where the MWD is the most sensitive among these three variables when the used grid is changed. The control has fewer water points (WS^{utms}_{multi4}, 108, 137 in Tab. 1), 79% and 83% less than the reference using an unstructured triangular grid with 0.125 °resolutions ($WS^{ut}_{0.125}$, 521, 911) and the traditional simulation using a structured grid with 0.0625 ° resolution ($WS^{s}_{0.0625}$, 1, 632, 638) in the whole domain, respectively. Then, WS^{utms}_{multi4} takes 0.63 hours (Fig. 13), saving about 70% and 98% of the calculation time compared to the reference $WS^{ut}_{0.125}$ (2.04 hours in Fig. 13) and the traditional simulation $WS^{s}_{0.0625}$ (33.79 hours in Fig. 3), respectively, when using the same computational resources (128 computing cores) and simulating the same time length (31 days). ~~With the same computational resources (128 computing cores) simulating the same time length (31 days), WS^{utms}_{multi4} takes 0.63 hours, saving about 70% of the calculational time compared to the reference $WS^{ut}_{0.125}$ (2.04 hours), as shown in Fig. 13. Therefore, t~~These results demonstrate that wave model WW3 using a coarse-resolution grid~~s~~ in deep water areas has a negligible effect on wave simulation accuracy in the annual mean, and ~~. I~~it takes a small fraction of the computational time, compared with that using an unstructured grid or ~~using the traditional~~ a structured grid with a uniform-fine resolution in the whole domain.

~~This efficient wave simulation using the unstructured triangular multiscale grid is beneficial to operational wave forecasting. It can give faster warnings to minimize losses of coastal residents when catastrophic waves occur (WS^{utms}_{multi4}, 0.63 hours in Fig. 13), compared with wave simulation using the traditional structured grid with the same fine spatial resolution ($WS^{s}_{0.0625}$, 33.79 hours in Fig. 3). At the same time, it has fewer water points (WS^{utms}_{multi4}, 107, 317 in Tab. 1), 79% and 93% less than the reference ($WS^{ut}_{0.125}$, 521, 911) and the traditional simulation ($WS^{s}_{0.0625}$, 1, 632, 638), respectively. In atmosphere-ocean-wave~~

~~coupled models, wave models using the unstructured triangular multiscale grid can reduce the integration time of the wave component and shorten the flux-exchange time at the air-sea interface, finally enhancing the calculational efficiency of coupled systems.~~ From the above detailed evaluation, we can conclude that a new wave modeling framework with a multiscale grid system can achieve the goals of less computational time consumption (Figs 3. and 13) and better wave simulation precision (Figs. 10, 11, and 12). Such efficient wave simulations are beneficial to operational wave forecasting. It can give faster warnings than before (wave prediction using a uniform-fine resolution grid) to minimize losses of coastal residents when catastrophic waves occur. It also can reduce the error generation and propagation caused by the boundary downscaling process, decrease complexity (compared with a multi-layer nesting simulation), and enhance the computation efficiency of wave components in atmosphere-ocean-wave coupled models. This ~~suggests~~ indicates that this new wave modeling framework will accelerate the pace of high-resolution Earth system models including ocean surface waves as a fast-response physical process at the air-sea interface.

~~From the above detailed evaluation, we can conclude that a new wave modeling framework with an unstructured multiscale grid system can achieve the goals of less computational time consumption and better wave simulation precision, compared with traditional wave simulations with uniform fine-gridding space. The applicability of this wave modeling framework is also verified by using two other wind forcings, including the ECMWF ERA-Interim dataset with 0.25° resolutions, and the Climate Forecast System Version 2 (CFSR2) from the National Centers for Environmental Prediction (NCEP) with 0.2° resolutions.~~

5 Summary and Discussions

This paper directly demonstrates that higher-resolution wave simulation can obtain a more accurate wave state, but it requires huge computational resources and has low computing efficiency. To deal with this situation, this paper designs a new wave modeling framework with a multiscale system. It has the following advantages.

(1) Minimizing the number of computational ~~fine~~ grids. The wave dispersion relation regulating the wave modeling process shows that ocean surface waves are sensitive/insensitive to topographic effects in shallow/deep water areas. Then, the relationship between water depth and half of the wavelength can be a criterion dividing shallow and deep water areas, which can decrease the number of fine/coarse grids in shallow/deep water areas as much as possible ~~to the greatest extent~~. This way is more advantageous when the ocean wave process is incorporated into Earth system models because it can shorten the added computational time considerably. ~~as much as possible when the ocean wave process is considered.~~

(2) Quantifying the match between grid resolution settings and wind signals. After a series of experiment evaluations, ~~T~~this paper gives some suggestions for designing unstructured multiscale grid systems in deep water areas to avoid over-smoothing wind signals and enhance computational efficiency. In active typhoon areas, westerly areas, and weak wind areas, the spatial resolution of multiscale grid systems is suggested to be 1, 2, and 4 times coarser than that of wind forcing, respectively.

(3) Having similar accuracy using different spatial propagation schemes. This wave modeling framework has a variable grid resolution in geographic space. Then ~~This paper compares~~ the performance of wave simulation using four propagation schemes (including CRD-N, CRD-PSI, CRD-FCT, and implicit N) in ~~geographic~~ this space is evaluated~~, including CRD-N, CRD-PSI, CRD-FCT, and implicit N~~. Results show that ~~F~~the four schemes have similar behavior in simulation accuracy, but the default CRD-N scheme takes the least computational time.

(4) Achieving efficient and high-precision wave simulation. Evaluations of ~~A~~a series of experiments ~~evaluations~~ show that the designed wave modeling framework can achieve the goals of enhancing wave simulation precision and saving computational costs. ~~In deep water areas,~~ Compared with using an unstructured grid ($WS^{ut}_{0.125}$, 0.125 ° in the whole domain), the wave model using the unstructured ~~triangular~~ multiscale grid (WS^{utms}_{multi3}, keeping a same resolution (0.125 °) in shallow water areas and varying resolution (0.5 ° and 1 °) in deep water areas) has very similar performance in simulation accuracy but decreases more than 8~~0~~1% of the computational time consumption ~~compared with using the unstructured triangular grid ($WS^{ut}_{0.125}$)~~. ~~In shallow water areas,~~ Compared with using a structured grid ($WS^{s}_{0.0625}$, 0.0625 ° in the whole domain), the wave model using the multiscale grid (WS^{utms}_{multi4}, keeping a same resolution (0.0625 °) in the South China Sea area and varying resolution (0.125 °, 0.5 °, and 1 °) in other areas) can obtain more accurate wave states and only takes 2% of the computational time ~~compared with using the structured grid ($WS^{s}_{0.0625}$)~~.

After establishing this powerful wave modeling framework, we will continue to conduct the following studies in the future.

~~(1) This framework can be constantly updated. For example, grid resolutions in coastal areas can be finer to better describe complex topography, and other factors affecting the grid setting in deep water areas, especially in typhoon areas, should be explored further.~~

~~(2) As HPC technology advances, the resolution of coastal grids will increase by up to hundreds of meters or even meters. It is urgent to improve the simulated ability of wave models in coastal areas. In particular, the physical mechanism and numerical scheme of wave models using multiscale grids should be improved.~~

~~(3) The spatial resolution between the available wind forcing and unstructured multiscale grids are often mismatched. The linear interpolation method used in wave models may lose a lot of wind energy into wave models. Then a more reasonable interpolation scheme should be explored.~~

(1) This framework can be constantly updated.

(a) To optimize multiscale grids. As HPC technology advances, a multiscale grid with ultra-high resolution (tens of meters or even meters) in coastal areas and gradually coarse towards the open ocean, eventually covering the global ocean is needed. There is a very flexible and automatic tool named OceanMesh2D (Roberts et al., 2019) to generate this multiscale grid, which won't take much time. In the process of grid generation, a quantitative relationship of spatial resolution between wind forcing and wave models is provided in this paper for reference.

(b) To further improve the computational efficiency. A powerful implicit scheme is recommended because it isn't restrained by the CFL condition compared with the commonly used explicit scheme. We can set relatively large and reasonable integration time steps to further save computational time. Moreover, the newly developed parallelization algorithm named domain decomposition (Abdolali et al. 2020) can greatly reduce the number of information exchanges between computing cores, compared with the old algorithm called card deck.

(c) To improve physical processes. The physical processes in current wave models are suitable for wave simulation on the scale of hundreds of meters or kilometers. It is urgent to improve the underestimated wave states in coastal areas in numerical simulation, and develop physical processes to enhance the simulation ability of wave models with the scale of tens of meters or even meters. In particular, the physical mechanism and numerical scheme of wave models using multiscale grids which is the mainstream should be improved.

(d) To optimize the interpolation method. A linear interpolation method in wave models is used to deal with this common phenomenon that the spatial resolution of wave models and external forcings is inconsistent. This way will over-smoothed wind energy, leading to underestimated wave energy and poor wave simulation accuracy. Then a more reasonable interpolation method should be explored to alleviate this situation.

(2) The applicability of this framework will be further validated.

(a) To validate using other wind forcings. The atmosphere reanalysis dataset ECMWF ERA5 is used to drive wave model WW3 with a multiscale grid in this paper. The applicability of this framework should be further verified using another common wind forcing, the Climate Forecast System Version 2 (CFSR2) from the National Centers for Environmental Prediction (NCEP) with 0.2 ° resolutions. Moreover, the wind from an ultra-high resolution coupled system which has the ability to describe the track and intensity of tropical cyclones should be used to verify the applicability of this framework in active typhoon areas.

(b) To validate in wave model SWAN. This paper systematically evaluates the framework in wave model WW3. Since wave model SWAN has similar modeling ideas and governing equations to wave model WW3, the quantitative relationship of spatial resolution between wave models and wind forcing obtained in WW3 is also applicable theoretically to SWAN. More detailed testing and evaluations will be done in the future. It should be noted that this framework is not suitable for the wave model WAM, for this model does not support unstructured triangular grids currently.

(~~4~~c) To validate in Earth system models. ~~Ocean surface waves can be~~ As an important physical process ~~to participate~~ at the air-sea interface, ocean surface waves should be incorporated into Earth system models. Usually, the significant wave feedback to the atmosphere and ocean is where the wave height is large, and these areas are already gridded with high-resolution model resolutions in this paper. A more detailed test of whether the wave feedback to air-sea interactions is related to wave model resolutions that have an inhomogeneity wave information will be further operated. After that, ~~S~~systematically evaluating the contribution of ocean surface waves to the atmospheric planetary boundary layer and upper-ocean mixing will be conducted. This will help us to deepen our understanding of ~~the~~ physical processes at the air-sea interface.

Code and data availability

The wave model WaveWatch III (WW3) used in this paper is from the Environmental Modeling Center (EMC), National Oceanic and Atmospheric Administration (NOAA), and its source code can be downloaded from the website: https://github.com/NOAA-EMC/WW3, last access: 9 February 2023. The Surface-water Modeling System software (SMS) for making unstructured triangular (multiscale) grid systems is available from the website: https://www.aquaveo.com/products, last access: 9 February 2023. The wind forcing is from the ERA5 dataset, European Center for Medium-Range Weather Forecasts (ECMWF) (website: https://cds.climate.copernicus.eu/cdsapp#!/dataset/reanalysis-era5-single-levels?tab=form, last access: 9 February 2023). The shoreline data is from the NOAA GSHHS dataset (website: https://www.ngdc.noaa.gov/mgg/shorelines/data/gshhg/, last access: 9 February 2023). The topography data comes from the NOAA ETOPO1 dataset (website: ~~https://www.ngdc.noaa.gov/mgg/global/global.html~~https://www.ngdc.noaa.gov/mgg/shorelines/gshhs.html, last access: 9 February 2023). The observation data can be downloaded from the National Marine Data Center, National Science & Technology Resource Sharing Service Platform of China (website: http://mds.nmdis.org.cn/, last access: 9 February 2023). Finally, the data used to produce the figures in this paper are available online (https:/doi.org/10.5281/zenodo.7827541~~7587673~~, last access: 9 February 2023) or by sending a written request to the corresponding author (Shaoqing Zhang, szhang@ouc.edu.cn).

Author contribution

Jiangyu Li designed the unstructured triangular multi-scale system, carried out all the experiments, and prepared the manuscript with contributions from all co-authors. Shaoqing Zhang provided the scientific idea~~,~~ and analy~~s~~zed the results with constructive discussions. Qingxiang Liu solved all the problems about wave models and checked carefully the words, figures, and tables of this manuscript. Xiaolin Yu and Zhiwei Zhang provided the test environment and intellectual discussion necessary for the model design.

Competing interests

The authors declare that they have no conflict of interest.

Acknowledgments

Many thanks to Dr. Jianguo Li from Met Office, United Kingdom, for his constructive comments and suggestions. This research is supported by the National Natural Science Foundation of China (41830964), the Shandong Province's "Taishan" Scientist Project (ts201712017), and the Qingdao Postdoctoral Applied Research Project.

References

Abdolali, A., Roland, A., van der Westhuysen, A., Meixner, J., Chawla, A., Hesser, T. J., Smith, J. M., and Sikiric, M. D.: Large-scale hurricane modeling using domain decomposition parallelization and implicit scheme implemented in WAVEWATCH III wave model, Coastal Engineering, 157, 103656, https:/doi.org/10.1016/j.coastaleng.2020.103656, 2020.

Bao, J. W., Wilczak, J. M., Choi, J. K., and Kantha, L. H.: Numerical simulations of air-sea interaction under high wind conditions using a coupled model: a study of Hurricane development, Monthly Weather Review, 128(7), 2190-2210, https:/doi.org/10.1175/1520-0493(2000)128<2190:NSOASI>2.0.CO;2, 2000.

Bao, Y., Song, Z. Y., and Qiao, F. L.: FIO-ESM version 2.0: model description and evaluation, Journal of Geophysical Research-Oceans, 125(6), e2019JC016036, https:/doi.org/10.1029/2019JC016036, 2020.

Brus, S. R., Wolfram, P. J., Van Roekel, L. P, and Meixner, J. D.: Unstructured global to coastal wave modeling for the Energy Exascale Earth System Model using WAVEWATCHIII version 6.07, Geoscientific Model Development, 14(5), 2917-2938, https:/doi.org/10.5194/gmd-14-2917-2021, 2021.

Cao, R. C., Chen, H. B., Rong, Z. R., and Lv, X. Q.: Impact of ocean waves on transport of underwater spilled oil in the Bohai Sea, Marine Pollution Bulletin, 171, 112702, https:/doi.org/10.1016/j.marpolbul.2021.112702, 2021.

Chawla, A., and Tolman, H. L.: Obstruction grids for spectral wave models, Ocean Modelling, 22(1-2), 12-25, https:/doi.org/10.1016/j.ocemod.2008.01.003, 2008.

Chen, X. Y., Ginis, I., and Hara, T.: Sensitivity of offshore tropical cyclone wave simulations to spatial resolution in wave models, Journal of Marine Science and Engineering, 6(4), 116, https:/doi.org/10.3390/jmse6040116, 2008.

Danabasoglu, G., Lamarque, J. F., Bacmeister, J., Bailey, D. A., Duvivier, A. K., Edwards, J., Danabasoglu, G., Lamarque, J. F., Bacmeister, J., Bailey, D. A., DuVivier, A. K., Edwards, J., Emmons, L. K., Fasullo, J., Garcia, R., Gettelman, A., Hannay, C., Holland, M. M., Large, W. G., Lauritzen, P. H., Lawrence, D. M., Lenaerts, J. T. M., Lindsay, K., Lipscomb, W. H., Mills, M. J., Neale, R., Oleson, K. W., Otto-Bliesner, B., Phillips, A. S., Sacks, W., Tilmes, S., van Kampenhout, L., Vertenstein, M., Bertini, A., Dennis, J., Deser, C., Fischer, C., Fox-Kemper, B., Kay, J. E., Kinnison, D., Kushner, P. J., Larson, V. E., Long, M. C., Mickelson, S., Moore, J. K., Nienhouse, E., Polvani, L., Rasch, P. J., and Strand, W. G.: The community Earth system model version 2 (CESM2), Journal of Advances in Modeling Earth Systems, 12(2), e2019MS001916, https:/doi.org/10.1029/2019MS001916, 2020.

Dunne, J. P., Horowitz, L. W., Adcroft, A. J., Ginoux, P., Held, I. M., John, J. G., Krasting, J. P., Malyshev, S., Naik, V., Paulot, F., Shevliakova, E., Stock, C. A., Zadeh, N., Balaji, V., Blanton, C., Dunne, K. A., Dupuis, C., Durachta, J., Dussin, R., Gauthier, P. P. G., Griffies, S. M., Guo, H., Hallberg, R. W., Harrison, M., He, J., Hurlin, W., McHugh, C., Menzel, R., Milly, P. C. D., Nikonov, S., J. Paynter, D., Ploshay, J., Radhakrishnan, A., Rand, K., Reichl, B. G., Robinson, T., Schwarzkopf, D. M., Sentman, L. T., Underwood, S., Vahlenkamp, H., Winton, M., Wittenberg, A. T., Wyman, B., Zeng, Y., and Zhao, M.: The GFDL Earth system model version 4.1 (GFDL-ESM 4.1): overall coupled model description and simulation characteristics, Journal of Advances in Modeling Earth Systems, 12(11), e2019MS002015, https:/doi.org/10.1029/2019MS002015, 2020.

Engwirda, D.: JIGSAW-GEO (1.0): locally orthogonal staggered unstructured grid generation for general circulation modelling on the sphere, Geoscientific Model Development, 10(6), 2117-2140, https:/doi.org/10.5194/gmd-10-2117-2017, 2017.

Feng, X. R., Yin, B. S., and Yang, D. Z.: Development of an unstructured-grid wave-current coupled model and its application, Ocean Modelling, 104, 213-225, https:/doi.org/10.1016/j.ocemod.2016.06.007, 2016.

Garg, N., Ng, E. Y. K., and Narasimalu, S.: The effects of sea spray and atmosphere–wave coupling on air–sea exchange during a tropical cyclone, Atmospheric Chemistry and Physics, 18(8), 6001-6021, https:/doi.org/10.5194/acp-18-6001-2018, 2018.

Higgins, C., Vanneste, J., and van den Bremer, T. S.: Unsteady Ekman-Stokes dynamics: implications for surface wave-induced drift of floating marine litter, Geophysical Research Letters, 47(18), e2020GL089189, https:/doi.org/10.1029/2020GL089189, 2020.

Hou, F., Gao, Z. Y., Li, J. G., and Yu, F. J.: An efficient algorithm for generating a spherical multiple-cell grid, Acta Oceanolologica Sinica, 41(5), 41-50, https:/doi.org/10.1007/s13131-021-1947-3, 2022.

Hsiao, S. C., Wu, H. L., Chen, W. B., Chang, C. H., and Lin, L. Y.: On the sensitivity of typhoon wave simulations to tidal elevation and current, Journal of Marine Science and Engineering, 8(9), 731, https:/doi.org/ 10.3390/jmse8090731, 2020.

Hughes, C. J., Liu, G. Q., Perrie, W., and Sheng, J. Y.: Impact of Langmuir turbulence, wave breaking, and Stokes drift on upper ocean dynamics under hurricane conditions, Journal of Geophysical Research-Oceans, 126(10), e2021JC017388, https:/doi.org/10.1029/2021JC017388, 2021.

Jiang, Y., Rong, Z. R., Li, P. X., Qin, T., Yu, X. L., Chi, Y. T., and Gao, Z. Y.: Modeling waves over the Changjiang River Estuary using a high-resolution unstructured SWAN model, Ocean Modelling, 173, 102007, https:/doi.org/10.1016/j.ocemod.2022.102007, 2022.

Jungclaus, J. H., Lorenz, S. J., Schmidt, H., Brovkin, V., Bruggemann, N., Chegini, F., Cruger, T., De-Vrese, P., Gayler, V., Giorgetta, M. A., Gutjahr, O., Haak, H., Hagemann, S., Hanke, M., Ilyina, T., Korn, P., Kroger, J., Linardakis, L., Mehlmann, C., Mikolajewicz, U., Muller, W. A., Nabel, J. E. M. S., Notz, D., Pohlmann, H., Putrasahan, D. A., Raddatz, T., Ramme, L., Redler, R., Reick, C. H., Riddick, T., Sam, T., Schneck, R., Schnur, R., Schupfner, M., von Storch, J. S., Wachsmann, F., Wieners, K. H., Ziemen, F., Stevens, B., Marotzke, J., and Claussen, M.: The ICON Earth system model version 1.0, Journal of Advances in Modeling Earth Systems, 14(4), e2021MS002813, https:/doi.org/10.1029/2021MS002813, 2022.

Kaiser, J., Nogueira, I. C. M., Campos, R. M., Parente, C. E., Martins, R. P., and Belo, W. C.: Evaluation of wave model performance in the South Atlantic Ocean: a study about physical parameterization and wind forcing calibration, Ocean Dynamics, 72(2), 137-150, https:/doi.org/10.1007/s10236-021-01495-4, 2022.

Li, J. G.: Global Transport on a Spherical Multiple-Cell Grid, Monthly Weather Review, 139(5), 1536-1555, https:/doi.org/10.1175/2010MWR3196.1, 2011.

Li, J. G.: Propagation of ocean surface waves on a spherical multiple-cell grid, Journal of Computational Physics, 231(24), 8262-8277, https:/doi.org/10.1016/j.jcp.2012.08.007, 2012.

Li, J. G., and Saulter, A.: Unified global and regional wave model on a multi-resolution grid, Ocean Dynamics, 64(11), 1657-1670, https:/doi.org/10.1007/s10236-014-0774-x, 2014.

Li, J. Y., and Zhang, S. Q.: Mitigation of model bias influences on wave data assimilation with multiple assimilation system using WaveWatch III v5.16 and SWAN v41.20, Geoscientific Model Development, 13(3), 1035-1054, https:/doi.org/10.5194/gmd-13-1035-2020, 2020.

Li, M. K., Zhang, S. Q., Wu, L. X., Lin, X. P., Chang, P., Danabasoglu, G., Wei, Z. Q., Yu, X. L., Hu, H. Q., Ma, X. H., Ma, W. W., Jia, D. N., Liu, X., Zhao, H. R., Mao, K., Ma, Y. W., Jiang, Y. J., Wang, X., Liu, G. L., and Chen, Y. X.: A high-resolution Asia-Pacific regional coupled prediction system with dynamically downscaling coupled data assimilation, Science Bulletin, 65(21), 1849-1858, https:/doi.org/10.1016/j.scib.2020.07.022, 2020.

Lin, Y. L., Huang, X. M., Liang, Y. S., Qin, Y., Xu, S. M., Huang, W. Y., Xu, F. H., Liu, L., Wang, Y., Peng, Y. R., Wang, L. N., Xue, W., Fu, H. H., Zhang, G. J., Wang, B., Li, R. Z., Zhang, C., Lu, H., Yang, K., Luo, Y., Bai, Y. Q., Song, Z. Y., Wang, M. Q., Zhao, W. J., Zhang, F., Xu, J. H., Zhao, X., Lu, C. S., Chen, Y. Z., Luo, Y. Q., Hu, Y., Tang, Q., Chen, D. X., Yang, G. W., and Gong, P.: Community integrated Earth system model (CIESM): description and evaluation, Journal of Advances in Modeling Earth Systems, 12(8), 1-29, https:/doi.org/10.1029/2019MS002036, 2020.

Liu, Q. X., Rogers, W. E., Babanin, A. V., Young, I. R., Romero, L., Zieger, S., Qiao, F. L., and Guan, C. L.: Observation-based source terms in the third-generation wave model WAVEWATCH III: Updates and verification, Journal of Physical Oceanography, 49(2), 489-517, https:/doi.org/10.1175/JPO-D-18-0137.1, 2019.

Mao, M. H., van der Westhuysen, A. J., Xia, M., Schwab, D. J., and Chawla, A.: Modeling wind waves from deep to shallow waters in Lake Michigan using unstructured SWAN, Journal of Geophysical Research: Oceans, 121(6), 3836-3865, https:/doi.org/10.1002/2015JC011340, 2015.

Mentaschi, L., Perez, J., Besio, G., Mendez, F. J., and Menendez, M.: Parameterization of unresolved obstacles in wave modelling: A source term approach, Ocean Modelling, 96, 93-102, https:/doi.org/10.1016/j.ocemod.2015.05.004, 2015.

Pallares, E., Lopez, J., Espino, M., and Sanchez-Arcilla, A.: Comparison between nested grids and unstructured grids for a high-resolution wave forecasting system in the western Mediterranean sea, Journal of operational oceanography, 10(1), 45-58, https:/doi.org/10.1080/1755876X.2016.1260389, 2017.

Qiao, F. L., Yuan, Y. L., Ezer, T., Xia, C. S., Yang, Y. Z., Lu, X. G., and Song, Z. Y.: A three-dimensional surface wave-ocean circulation coupled model and its initial testing, Ocean Dynamics, 60(5), 1339-1355, https:/doi.org/10.1007/s10236-010-0326-y, 2010.

Roberts, K. J., Pringle, W. J., and Westerink, J. J.: OceanMesh2D 1.0: MATLAB-based software for two-dimensional unstructured mesh generation in coastal ocean modelling, Geoscientific Model Development, 12(5), 1847-1868, https:/doi.org/10.5194/gmd-12-1847-2019, 2019.

Rogers, W. E., and Campbell, T. J.: Implementation of curvilinear coordinate system in the WAVEWATCH III model, NRL Memorandum Report NRL/MR/7320–09-9193, Naval Research Laboratory, Stennis Space Center, MS 39529-55004, 42 pp., 2009.

Rogers, W. E., and Holland, K. T.: A study of dissipation of wind-waves by mud at Cassino Beach, Brazil: Prediction and inversion, Continental Shelf Research, 29(3), 676-690, https:/doi.org/10.1016/j.csr.2008.09.013, 2009.

Roland, A., and Ardhuin, F.: On the developments of spectral wave models: numerics and parameterizations for the coastal ocean, Ocean Dynamics, 64, 833-846, https:/doi.org/10.1007/s10236-014-0711-z, 2014.

Roland, A.: Development of WWM II: Spectral Wave Modelling on Unstructured Meshes, Ph.D. thesis, Institut für Wasserbau und Wasserwirtschaft, Technische University Darmstadt, Germany, 35 pp., 2009.

Roland, A., Cucco, A., Ferrarin, C., Hsu, T. W., Liau, J. M., Ou, S. H., Umgiesser, G., and Zanke, U.: On the development and verification of a 2-D coupled wave-current model on unstructured meshes, Journal of Marine Systems, 78, S244-S254, https:/doi.org/10.1016/j.jmarsys.2009.01.026, 2009.

Sikiric, M., D., Ivankovic, D., Roland, A., Ivatek-Sahdan, S., and Tudor, M.: Operational wave modelling in the Adriatic Sea with the wind wave model, Pure and Applied Geophysics, 175(11), 3801-3815, https://doi.org/10.1007/s00024-018-1954-2, 2018.

Stopa, J. E., Ardhuin, F., Babanin, A., and Zieger, S.: Comparison and validation of physical wave parameterizations in spectral wave models, Ocean Modelling, 103, 2-17, https:/doi.org/10.1016/j.ocemod.2015.09.003, 2016.

Sullivan, P. P., and McWilliams, J. C.: Dynamics of winds and currents coupled to surface waves, Annual Review of Fluid Mechanics, 42, 19-42, https:/doi/org/10.1146/annurev-fluid-121108-145541, 2010.

Tao, A. F., Shen, Z. C., Li, S., Xu, X., and Zhang, Y.: Research progress for disastrous waves in China, Science & Technology Review, 36(14), 26-34, https:/doi.org/10.3981/j.issn.1000-7857.2018.14.005, 2018.

Tolman, H. L.: A Third-Generation Model for Wind Waves on Slowly Varying, Unsteady, and Inhomogeneous Depths and Currents, Journal of Physical Oceanography, 21(6), 782-797, https:/doi.org/10.1175/1520-0485(1991)021<0782:ATGMFW>2.0.CO;2, 1991.

Tolman, H. L.: Treatment of unresolved islands and ice in wind wave models, Ocean Modelling, 5(3), 219-231, https:/doi.org/10.1016/S1463-5003(02)00040-9, 2003.

WAMDI Group: The WAM model-a third generation ocean wave prediction model, Journal of Physical Oceanography, 18(12), 1775-1810, https:/doi.org/10.1175/1520-0485(1988)018<1775:TWMTGO>2.0.CO;2, 1988.

Wu, W. F., Li, P. L., Zhai, F. G., Gu, Y. Z., and Liu, Z. Z.: Evaluation of different wind resources in simulating wave height for the Bohai, Yellow, and East China Seas (BYES) with SWAN model, Continental Shelf Research, 207, 104217, https:/doi.org/10.1016/j.csr.2020.104217, 2020.

WW3DG: User manual and system documentation of WAVEWATCH III version 6.07, the WAVEWATCH III Development Group. Tech. Note 316. NOAA/NWS/NCEP/MMAB, 2019.

Wu, Z. Y., Chen, J., Jiang, C. B., and Deng, B.: Simulation of extreme waves using coupled atmosphere-wave modeling system over the South China Sea, Ocean Engineering, 221, 108531, https:/doi.org/10.1016/j.oceaneng.2020.108531, 2021.

Xu, Y., He, H. L., Song, J. B., Hou, Y. J., and Li, F. N.: Observations and modeling of typhoon waves in the South China Sea, Journal of Physical Oceanography, 47(6), 1307-1324, https:/doi.org/10.1175/JPO-D-16-0174.1, 2017.

Yang, Y. Z., Qiao, F. L., Zhao, W., Teng, Y., and Yuan, Y. L.: MASNUM ocean wave numerical model in spherical coordinates and its application, Acta Oceanologica Sinica, 27(2), 1-7, https:/doi.org/10.3321/j.issn:0253-4193.2005.02.001, 2005.

Zhang, L. X., Zhang, X. F., Perrie, W., Guan, C. L., Dan, B., Sun, C. J., Wu, X. R., Liu, K. X., and Li, D.: Impact of sea spray and sea surface roughness on the upper ocean response to super typhoon Haitang (2015), Journal of Physical Oceanography, 51(6), 1929-1945, https:/doi.org/10.1175/JPO-D-20-0208.1, 2021.

Zhang, X. F., Han, G. J., Wang, D. X., Deng, Z. G., and Li, W.: Summer surface layer thermal response to surface gravity waves in the Yellow Sea, Ocean Dynamics, 62(7), 983-1000, https:/doi.org/10.1007/s10236-012-0547-3, 2012.

Zieger, S., Babanin, A. V., Rogers, W. E., and Yong, I. R.: Observation-based source terms in the third-generation wave model WAVEWATCH, Ocean Modeling, 96, 2-25, https:/doi.org/10.1016/j.ocemod.2015.07.014, 2015.

Ziehn T., Chamberlain M. A., Law R. M., Lenton, A., Bodman, R. W., Dix, M., Stevens, L., Wang, Y. P., and Srbinovsky, J.: The Australian Earth system model: ACCESS-ESM1.5, Journal of Southern Hemisphere Earth System Science, 70(1), 193-214, https://doi.org/10.1071/ES19035, 2020.

Zijlema, M.: Computation of wind-wave spectra in coastal waters with SWAN on unstructured grids, Coastal Engineering, 57(3), 267-277, https:/doi.org/10.1016/j.coastaleng.2009.10.011, 2010.

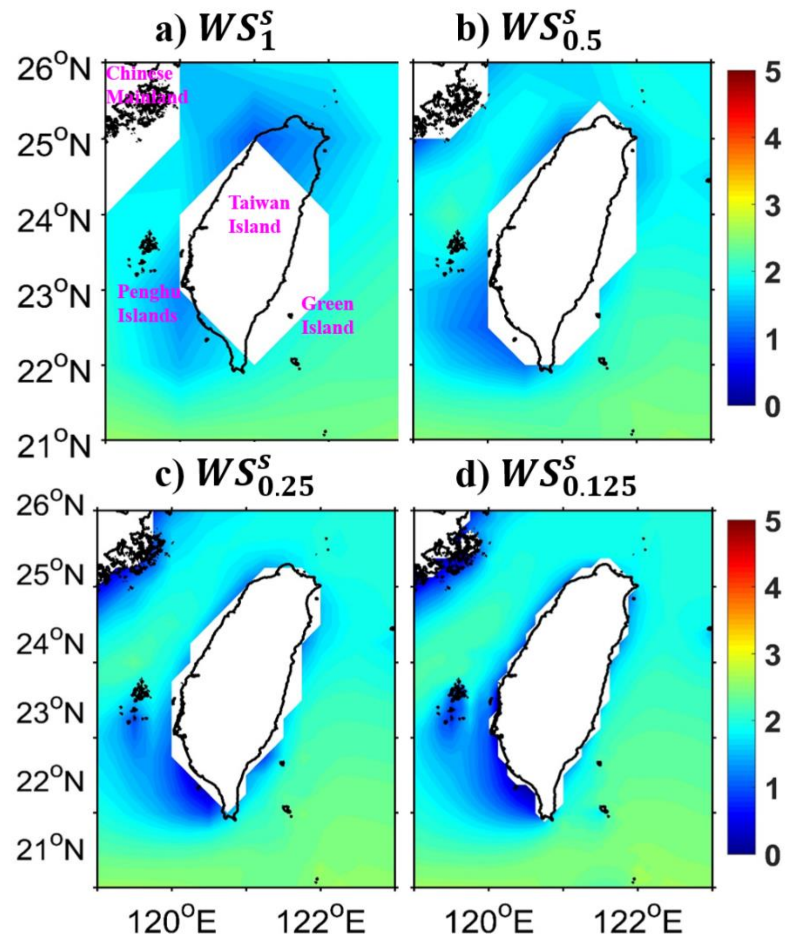

Figure 1: Spatial distributions of significant wave heights (SWHs) from wave simulation (briefly as "WS") using a traditional structured grid system (briefly as "s" in the superscript) with a) 1°, b) 0.5°, c) 0.25°, and d) 0.125° model resolutions (denoted as the subscript) around Taiwan Island, China in January 2018, called WS^s_1, $WS^s_{0.5}$, $WS^s_{0.25}$, and $WS^s_{0.125}$ (see Tab. 1), respectively (unit: meter). The color-shaded and white indicate the ocean and land identified in wave model WW3 with different resolutions. The areas surrounded by black lines (from the NOAA GSHHS dataset) generally represent the real lands.

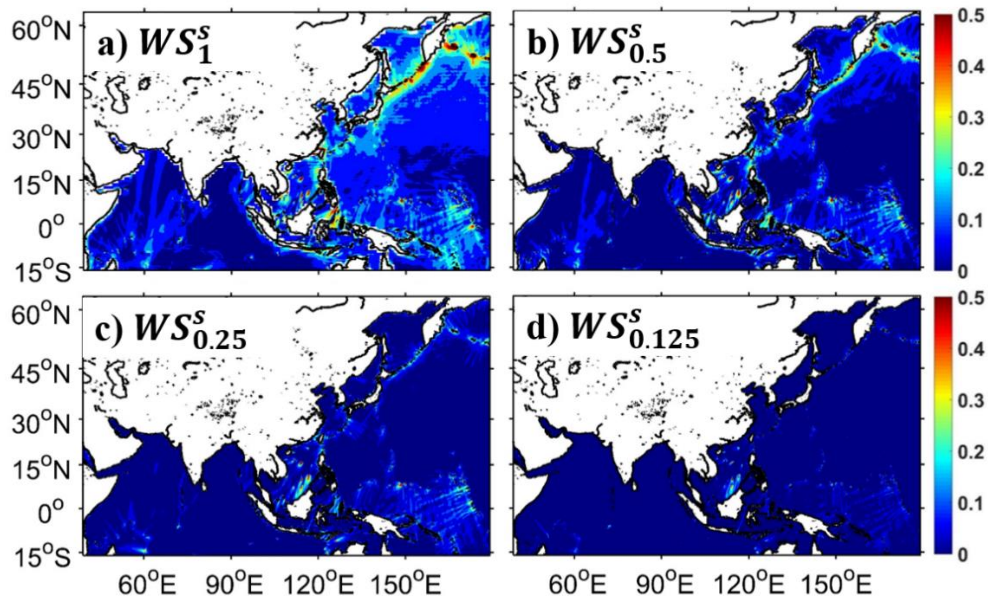

Figure 2: Spatial distributions of SWH root mean square differences (RMSDs) from a) WS_1^s, b) $WS_{0.5}^s$, c) $WS_{0.25}^s$, and d) $WS_{0.125}^s$ around the Asia-Pacific area in January 2018 (unit: meter). The $WS_{0.0625}^s$ in Tab. 1 is considered as a reference to calculate four SWH RMSDs by linear interpolation.

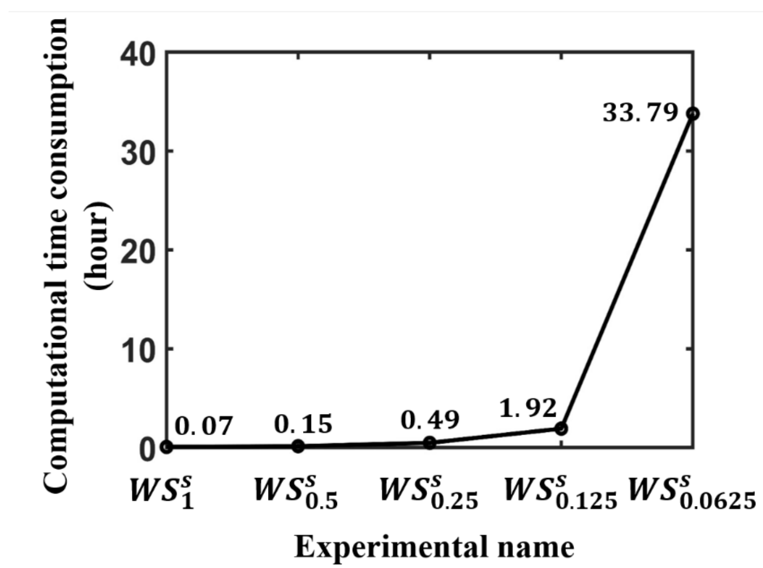

Figure 3: The computational time consumption from WS_1^s, $WS_{0.5}^s$, $WS_{0.25}^s$, $WS_{0.125}^s$, and $WS_{0.0625}^s$ using the same computational resources (128 computing cores) to simulate one-month (January 2018) wave states around the Asia-Pacific area. The specific time consumption is listed at the corresponding position.

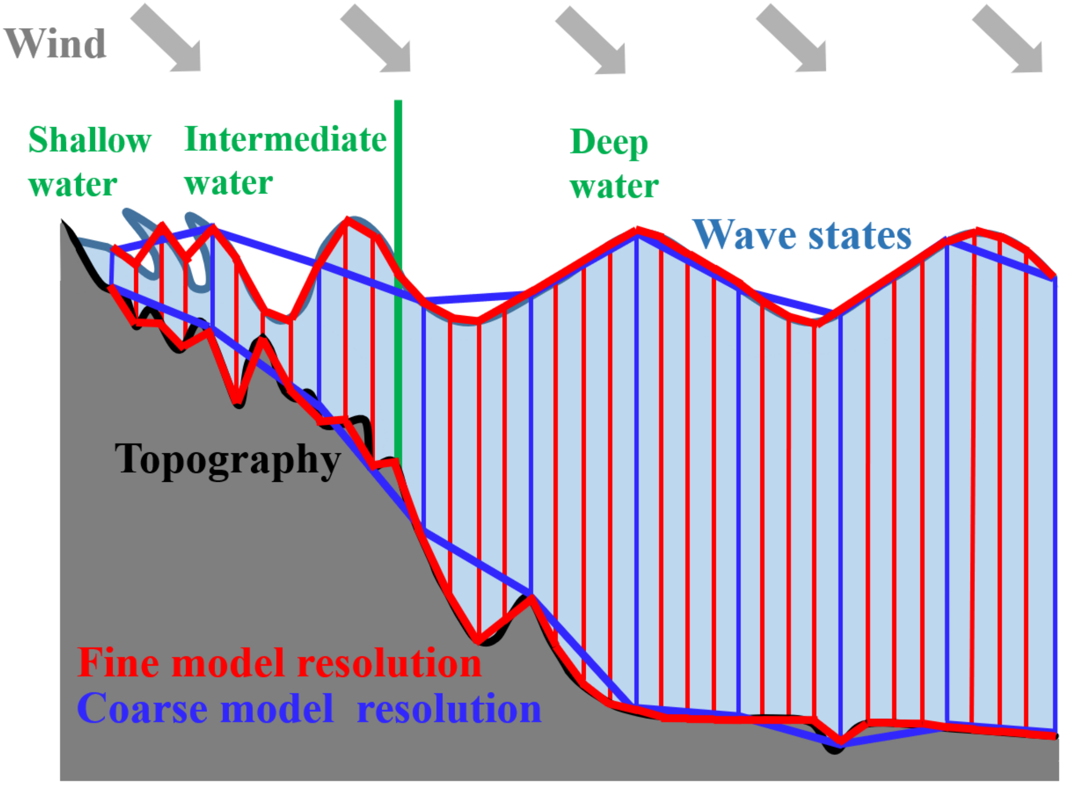
Wind
Shallow water
Intermediate water
Deep water
Wave states
Topography
Fine model resolution
Coarse model resolution

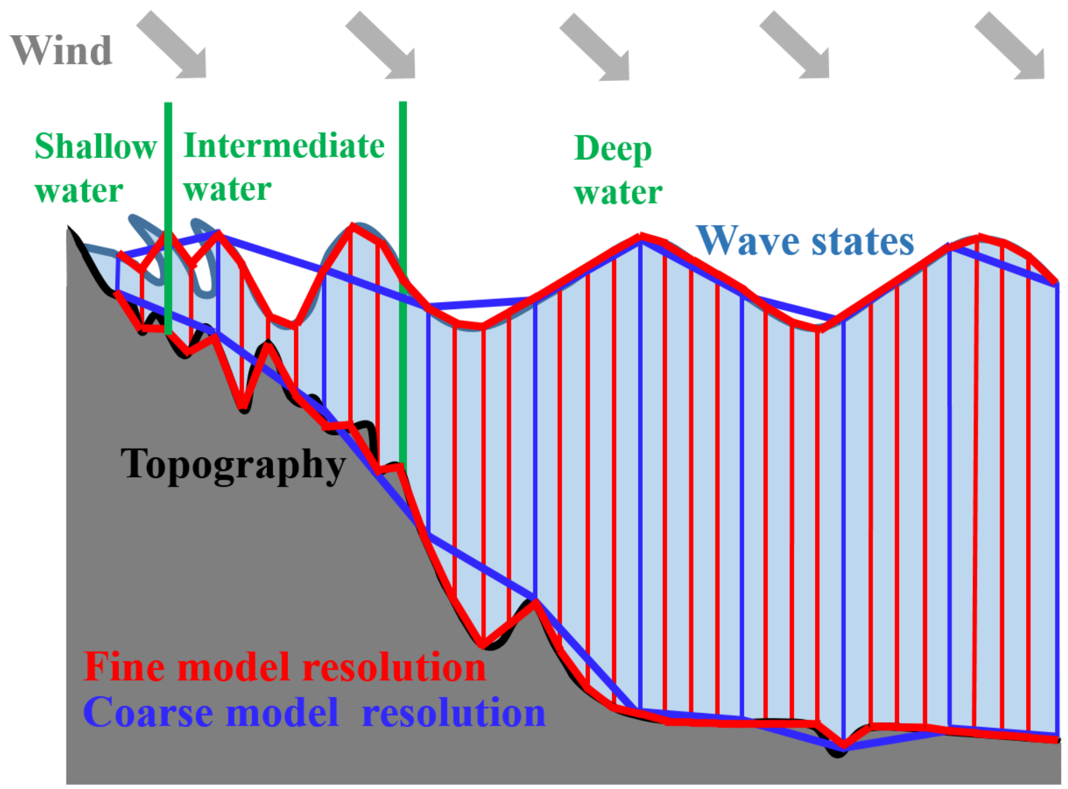

Figure 4: A schematic diagram of wave models describing complex topographic features (grey fill) and simulating wave states (navy-blue lines) using fine (red lines) and coarse (blue lines) model resolutions in shallow, intermediate, and deep water areas (~~left and right of the~~using green vertical bars as dividing lines). The black and navy-blue lines represent the actual land-ocean boundary and wave states, which are described with the thick red and blue lines in wave models. Note that this figure does not represent the actual wave modeling process and the spatial scale of ocean surface waves.

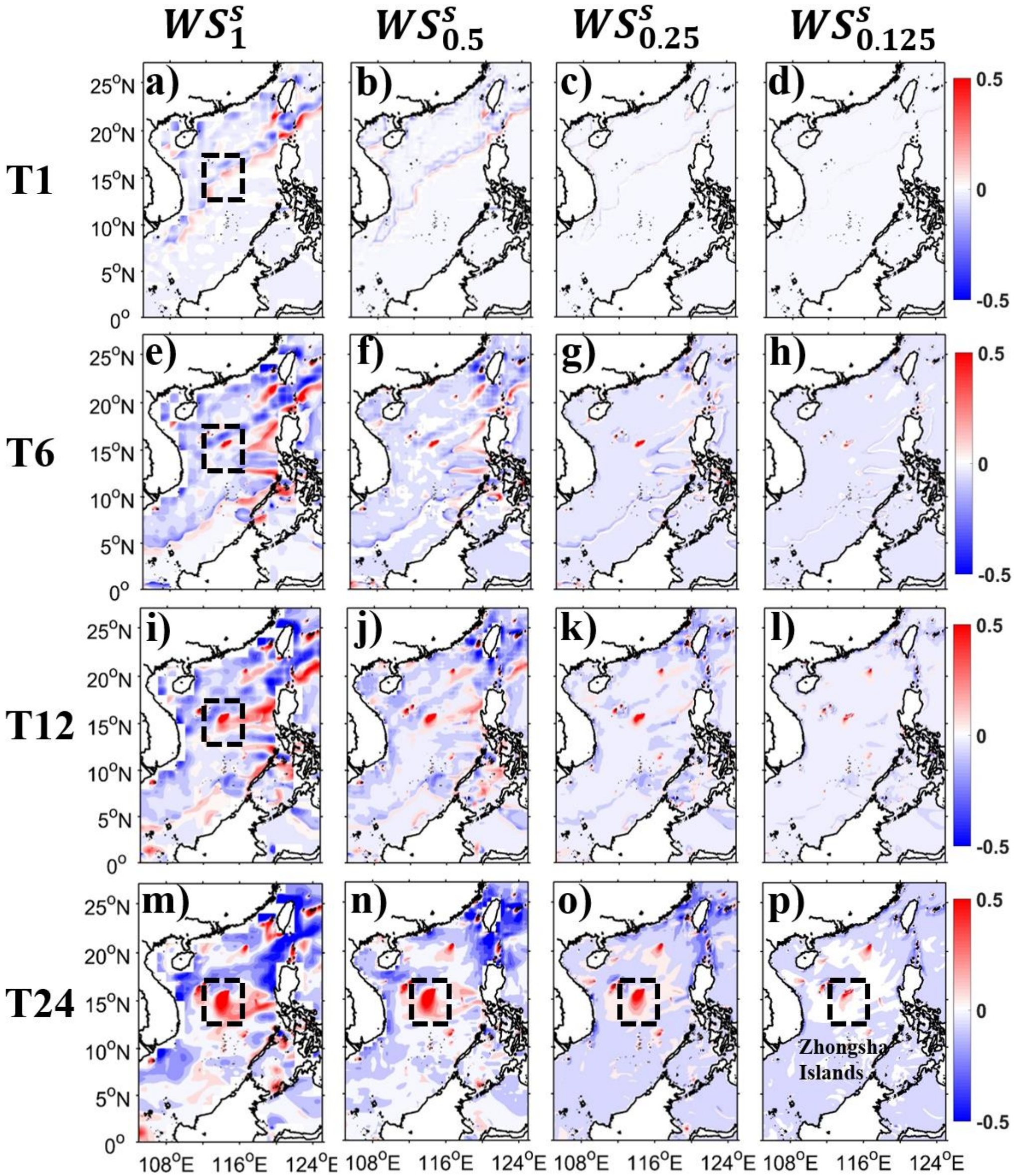

WS_1^s
$WS_{0.5}^s$
$WS_{0.25}^s$
$WS_{0.125}^s$
T1
T6
T12
T24
a)
b)
c)
d)
e)
f)
g)
h)
i)
j)
k)
l)
m)
n)
o)
p)
25°N
20°N
15°N
10°N
5°N
0°
108°E
116°E
124°E
0.5
0
-0.5
Zhongsha
Islands

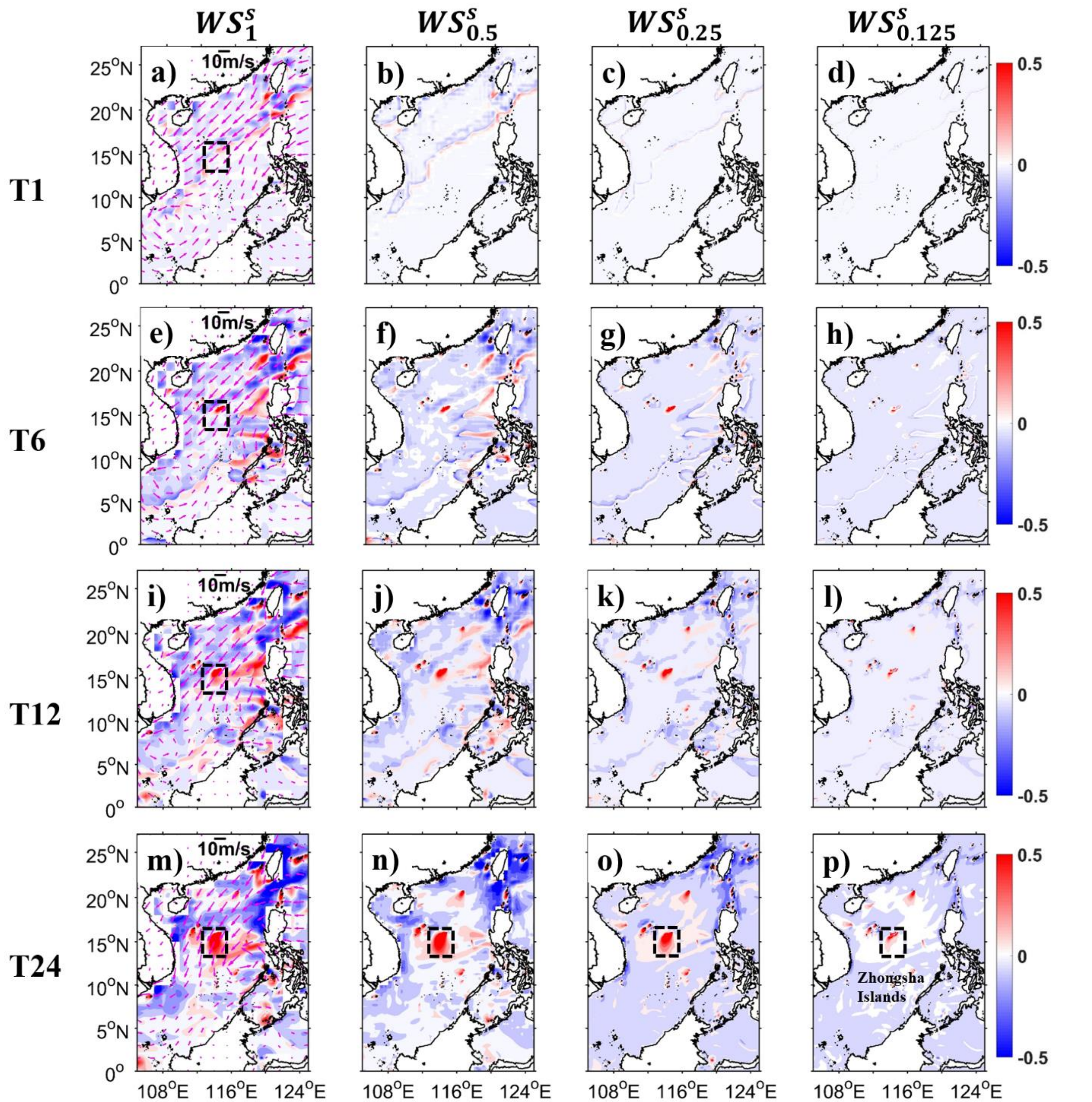

Figure 5: Spatial distributions of SWH differences from WS_1^s (a, e, i, m), $WS_{0.5}^s$ (b, f, j, n), $WS_{0.25}^s$ (c, g, k, o), and $WS_{0.125}^s$ (d, h, l, p) around the South China Sea at 01:00, 06:00, 12:00 UTC, November 1, 2017 (the first, second, third row, named T1, T6, T12), and 00:00 UTC, November 2, 2017 (the fourth row, named T24) (note that the wave states of all experiments at 00:00 UTC, November 1, 2017, are resting) (unit: meter). The magenta arrows in the first column (a, e, i, m) are wind vectors for the corresponding moment (unit: m/s). The Zhongsha Islands are circled by dashed boxes in the first column and the last row. The $WS_{0.0625}^s$ in Tab. 1 is considered as a reference to calculate SWH differences by linear interpolation (interpolated results minus the reference).

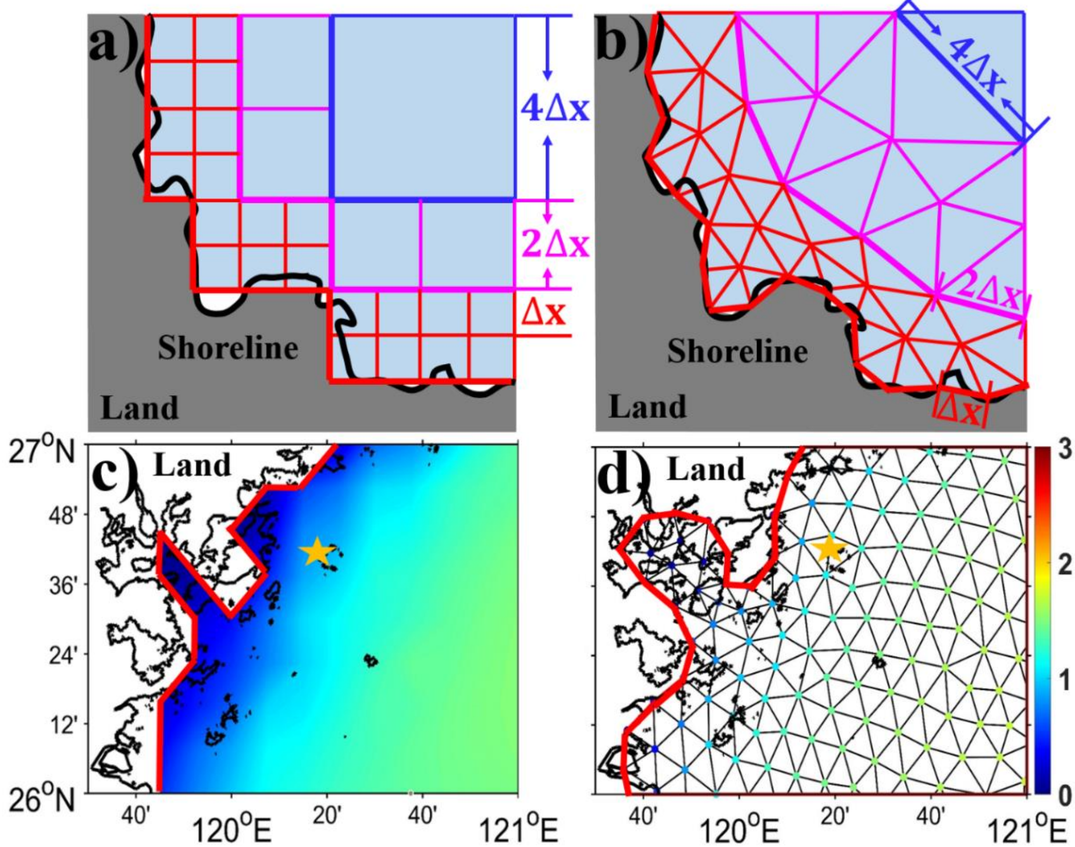

Figure 6: A diagram of unstructured a) rectangular and b) triangular multiscale grid systems with Δx, 2Δx, and 4Δx spatial resolutions in shallow, transitional, and deep water areas marked with red, magenta, and blue lines. Spatial distributions of SWHs are from wave simulation using c) traditional structured grid and d) unstructured triangular grid both with a fine resolution (named $WS^{s}_{0.125}$ and $WS^{ut}_{0.125}$ in Tab. 1) in July 2018 (unit: meter). The Chinese oceanic station named BSG is located at (120.3 °E, 26.7 °N) marked with yellow stars in c) and d). The thick black and red lines are actual and described land-ocean boundaries in four panels.

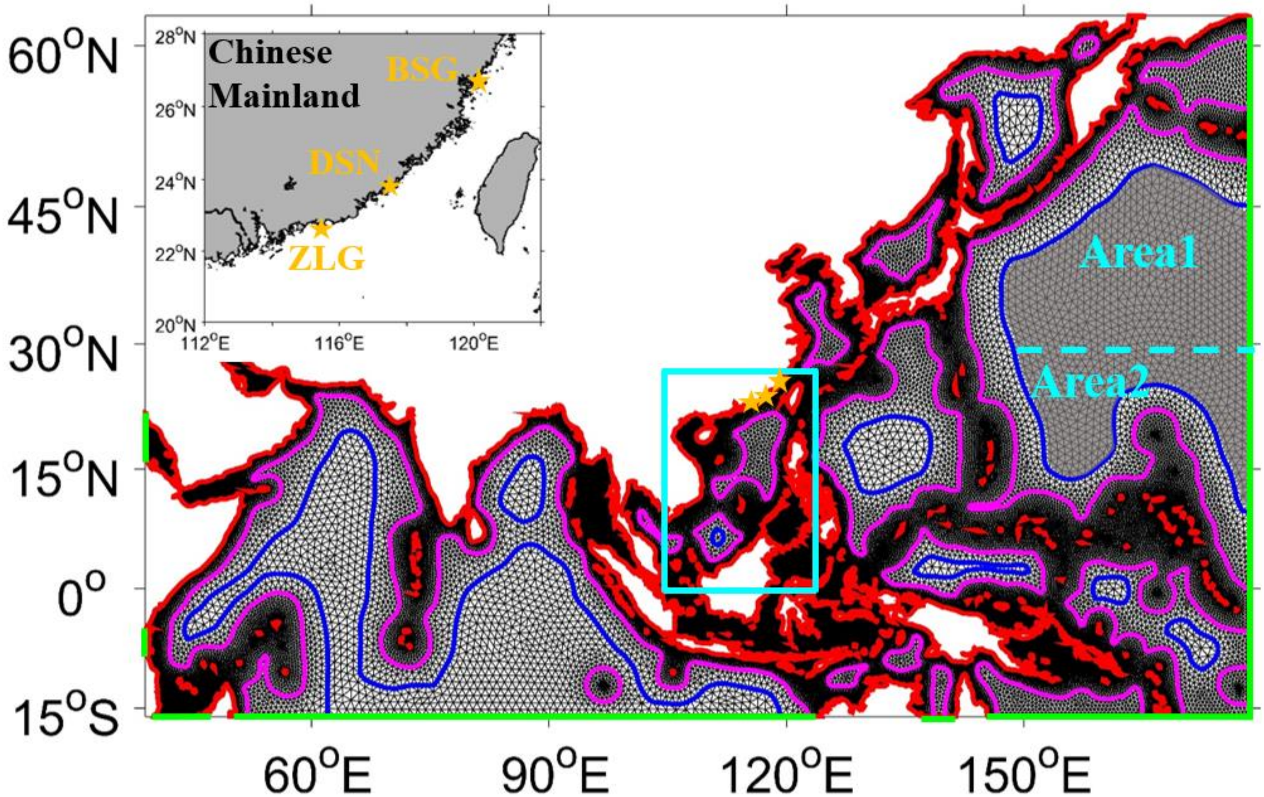

Figure 7: The spatial distribution of the new wave modeling framework using an unstructured triangular multiscale grid system. Grid resolutions vary from 0.125° in shallow water areas to 0.5° in transitional water areas and then to 1° in deep water areas, with the help of the shorelines (red) and two types of control lines (magenta and blue), named WS_{multi3}^{utms} in Tab. 1. The green lines represent spatial locations of the open boundary. The Chinese oceanic stations named BSG (same station in Fig. 6), DSN, and ZLG are marked with yellow stars, and the top-left panel is a clearer display. In the following section 4, this framework will be further developed in two areas. The first is the northern Pacific Ocean area with a grey fill (surrounded by a blue line) ($WS_{multi3(\mathrm{new})}^{utms}$). The second is around the South China Sea area circled by a cyan solid box (WS_{multi4}^{utms}). Please, see the corresponding part for details.

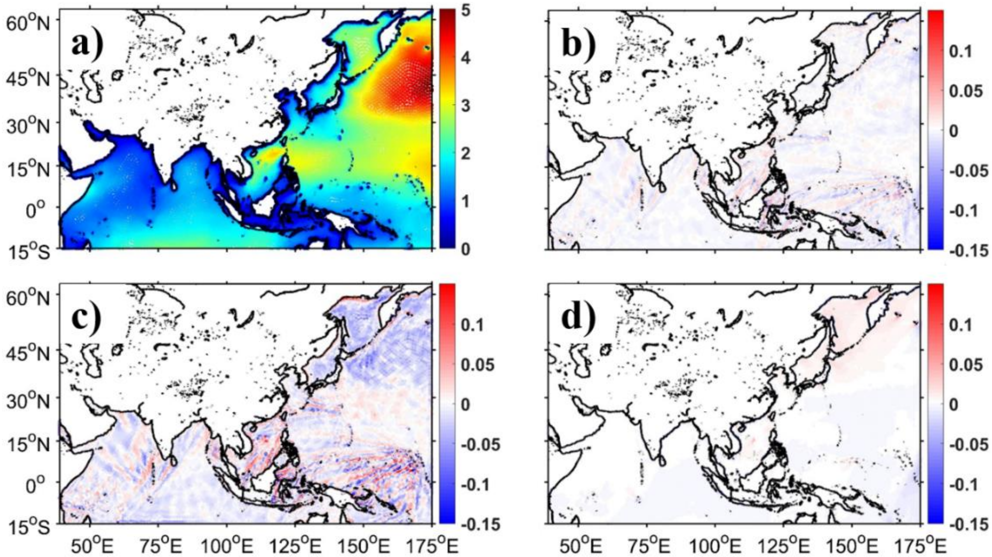

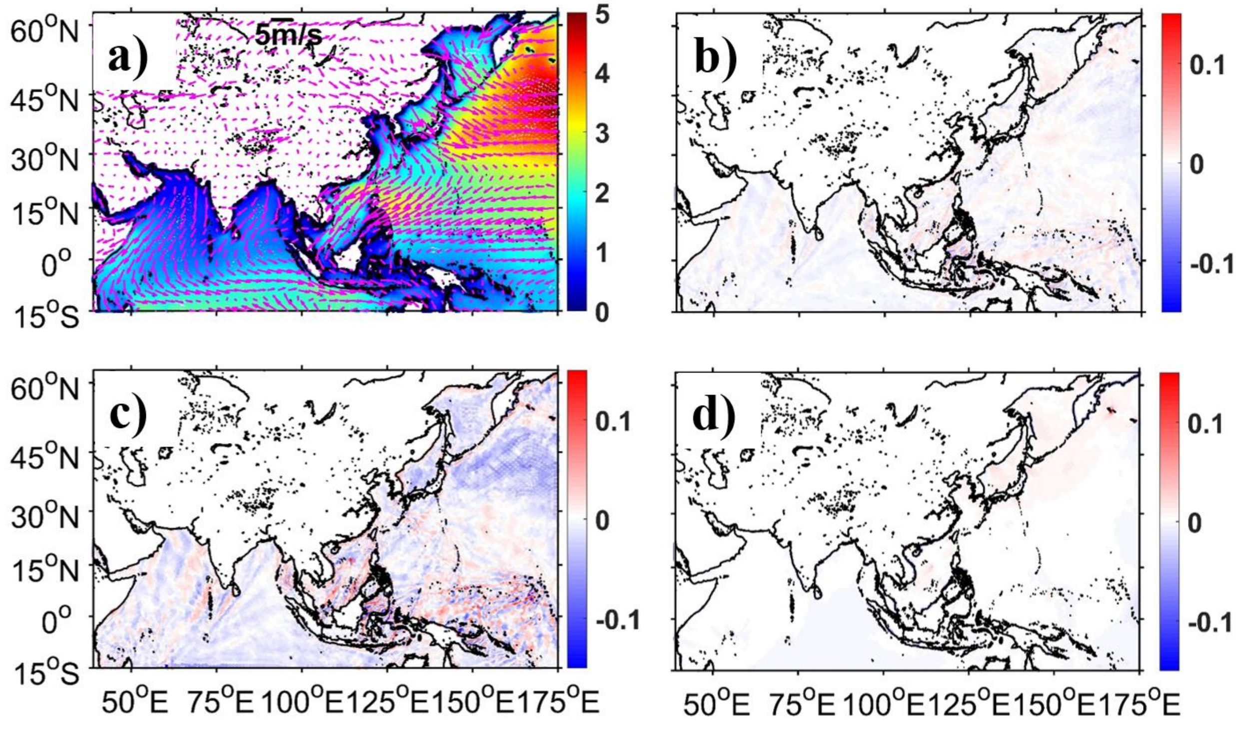

Figure 8: a) Spatial distributions of SWH from WS_{multi3}^{utms} using CRD-N propagation scheme and monthly-mean wind vectors (magenta arrows) in January 2018 (unit: meter for SWH, and m/s for wind vectors). b-d) Spatial distributions of SWH differences from WS_{multi3}^{utms} using CRD-PSI, CRD-FCT, and implicit N propagation schemes minus that using CRD-N scheme (Fig. 8a), respectively (unit: meter).

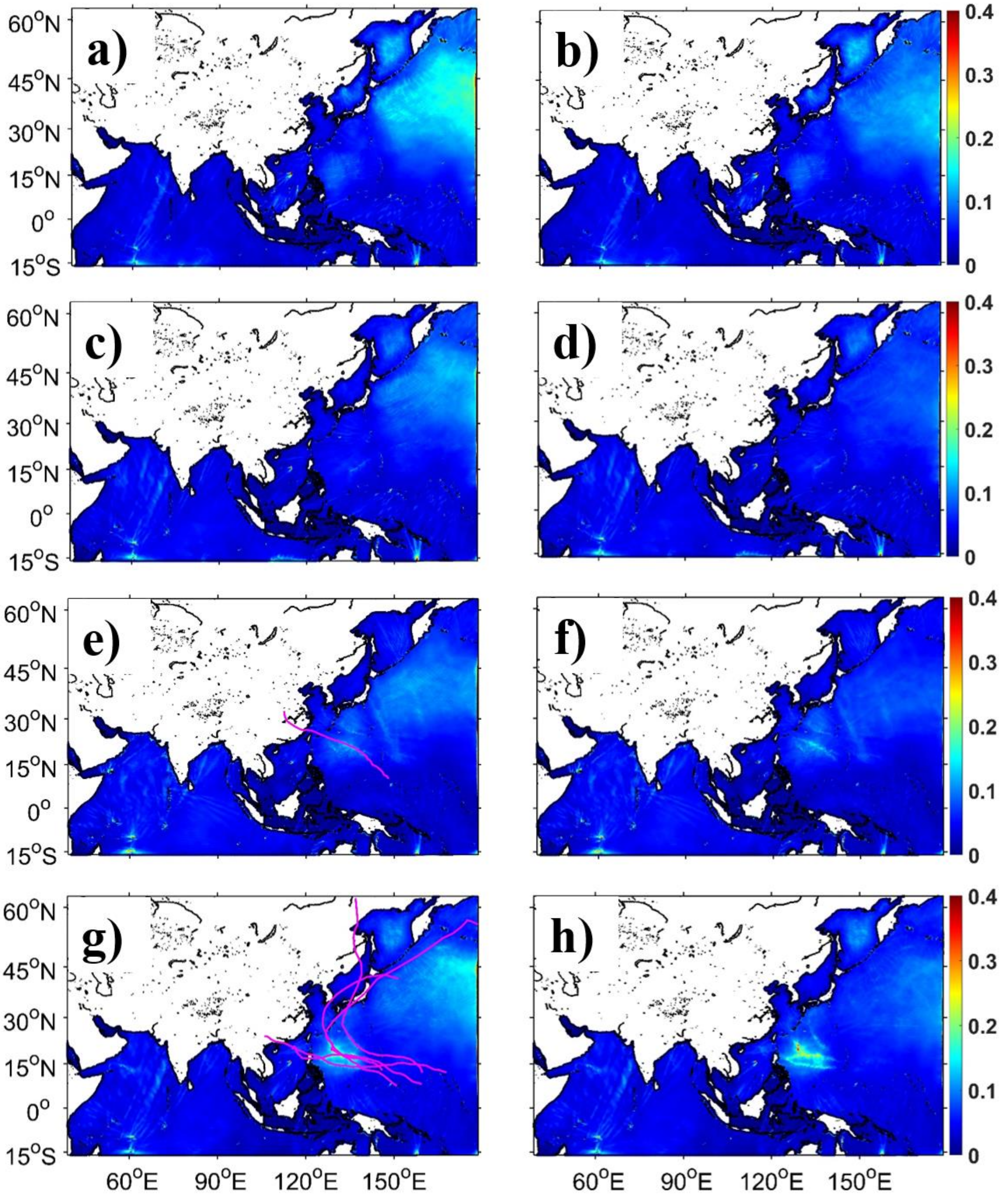
a)
b)
c)
d)
e)
f)
g)
h)
60°N
45°N
30°N
15°N
0°
15°S
60°E
90°E
120°E
150°E
0.4
0.3
0.2
0.1
0

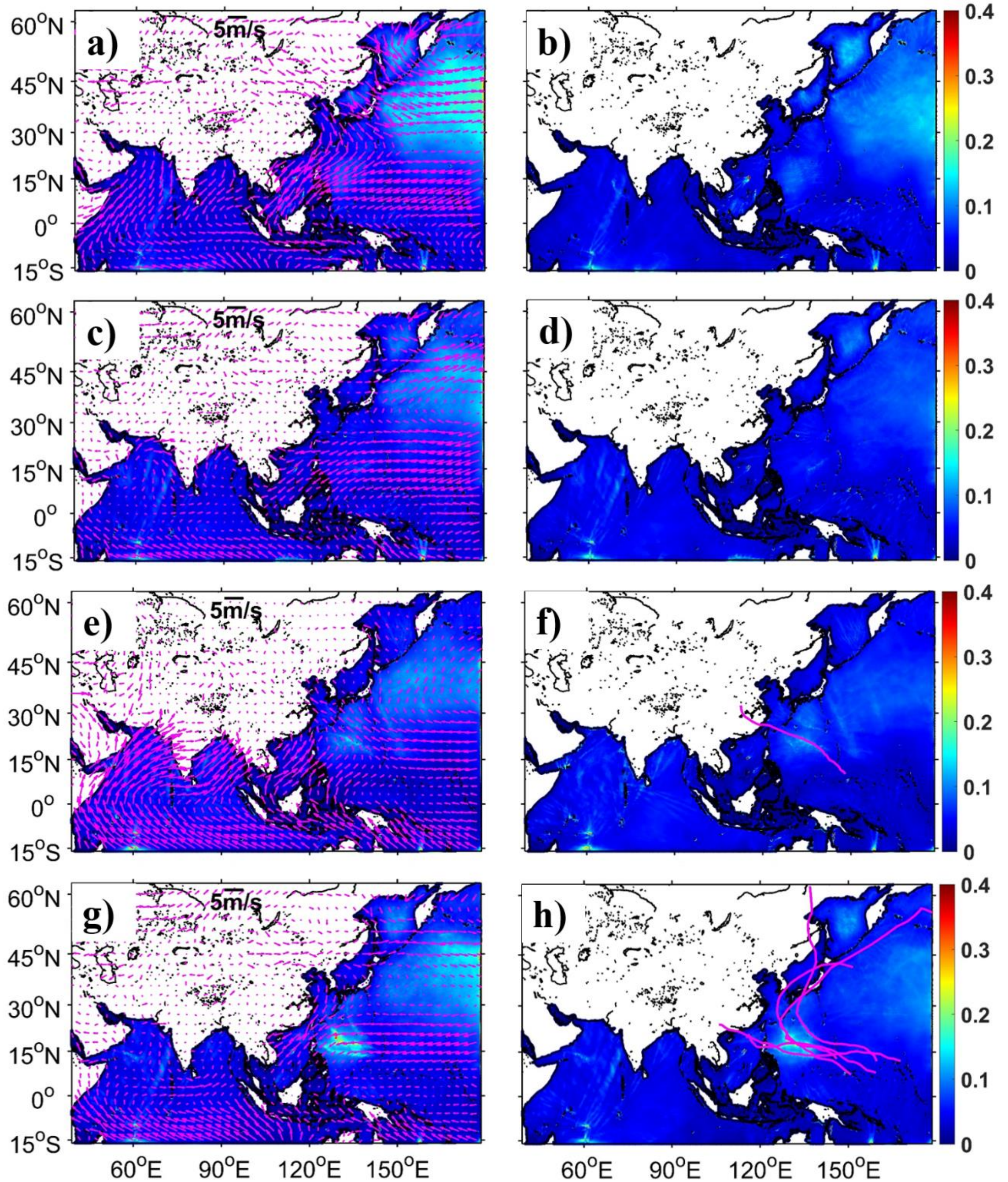

Figure 9: Spatial distributions of SWH RMSDs from WS_{multi3}^{utms} (a, c, e, g) and $WS_{multi3(\mathrm{new})}^{utms}$ (b, d, f, h) in the boreal winter (a, b), spring (c, d), summer (e, f), and autumn (g, h) of 2018 (unit: meter). The reference $WS_{0.125}^{ut}$ is used to calculate SWH RMSDs by linear interpolation. The magenta arrows in the left panels (a, c, e, g) are the average wind vectors in every season (unit: m/s). In panels f and h, the locations of large simulation differences coincide with partial tracks of some typhoons, which are shown with magenta lines. ~~The magenta lines in panels e and g are best tracks of some typhoons, which overlap the locations of large differences partially.~~

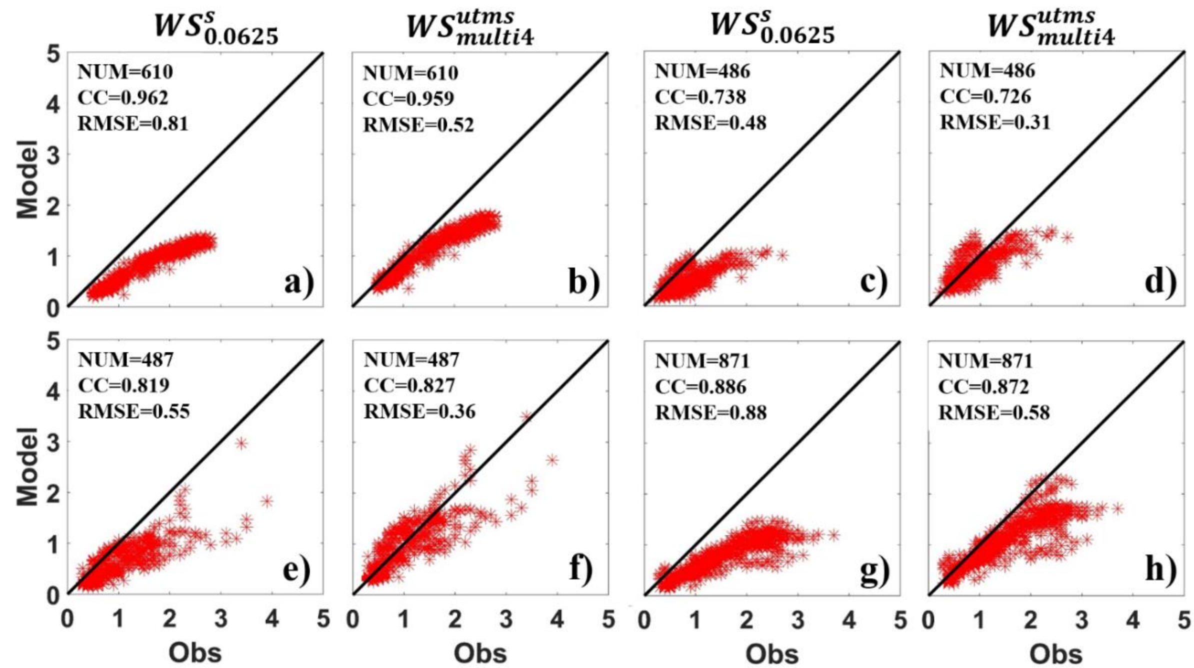

Figure 10: Scattered distributions of SWHs from $WS^{s}_{0.0625}$ (a, c, e, g) and WS^{utms}_{multi4} (b, d, f, h) at the observational station BSG (marked with yellow stars in Figs. 6 and 7) in the boreal winter (a, b), spring (c, d), summer (e, f), and autumn (g, h) of 2018 (unit: meter). The black lines in every panel indicate the best fit between wave simulation results (the vertical axis) and observations (the horizontal axis). The number of valid observations and the calculated SWH root mean square errors (RMSEs) and CCs are listed in the upper-left corner of every panel.

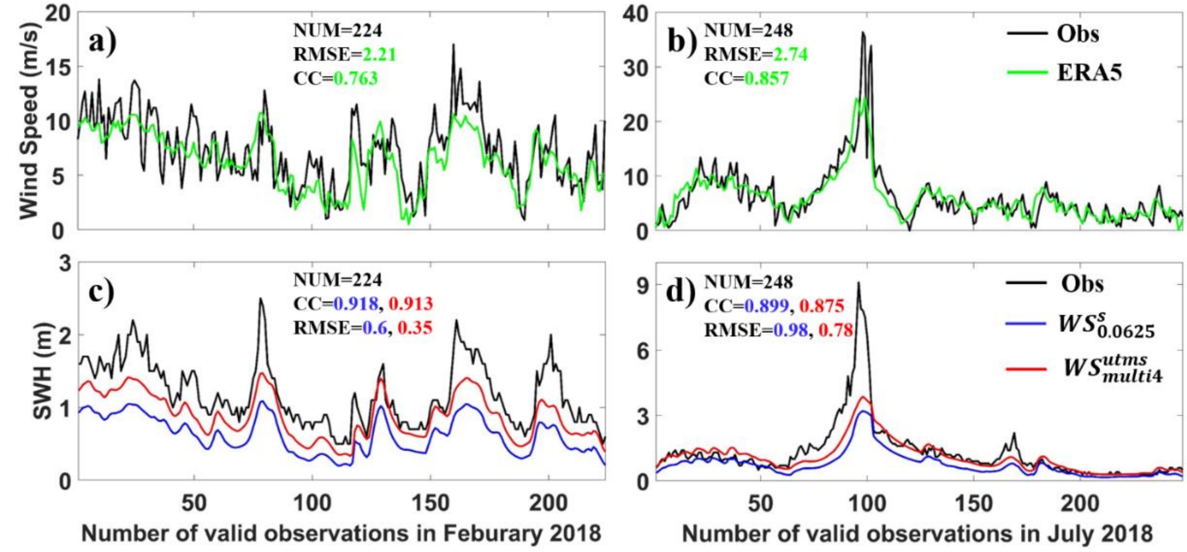

Figure 11: Time series of wind speeds (a, b) and SWHs (c, d) at the BSG observation station in boreal February (a, c) and July (b, d), 2018. Wind speeds and SWHs observed are plotted with black lines. The wind forcing is from the reanalysis dataset ERA5 plotted with green lines in a) and b). The simulated SWHs from $WS^{s}_{0.0625}$ and WS^{utms}_{multi4} are plotted with blue and red lines in c) and d), respectively.

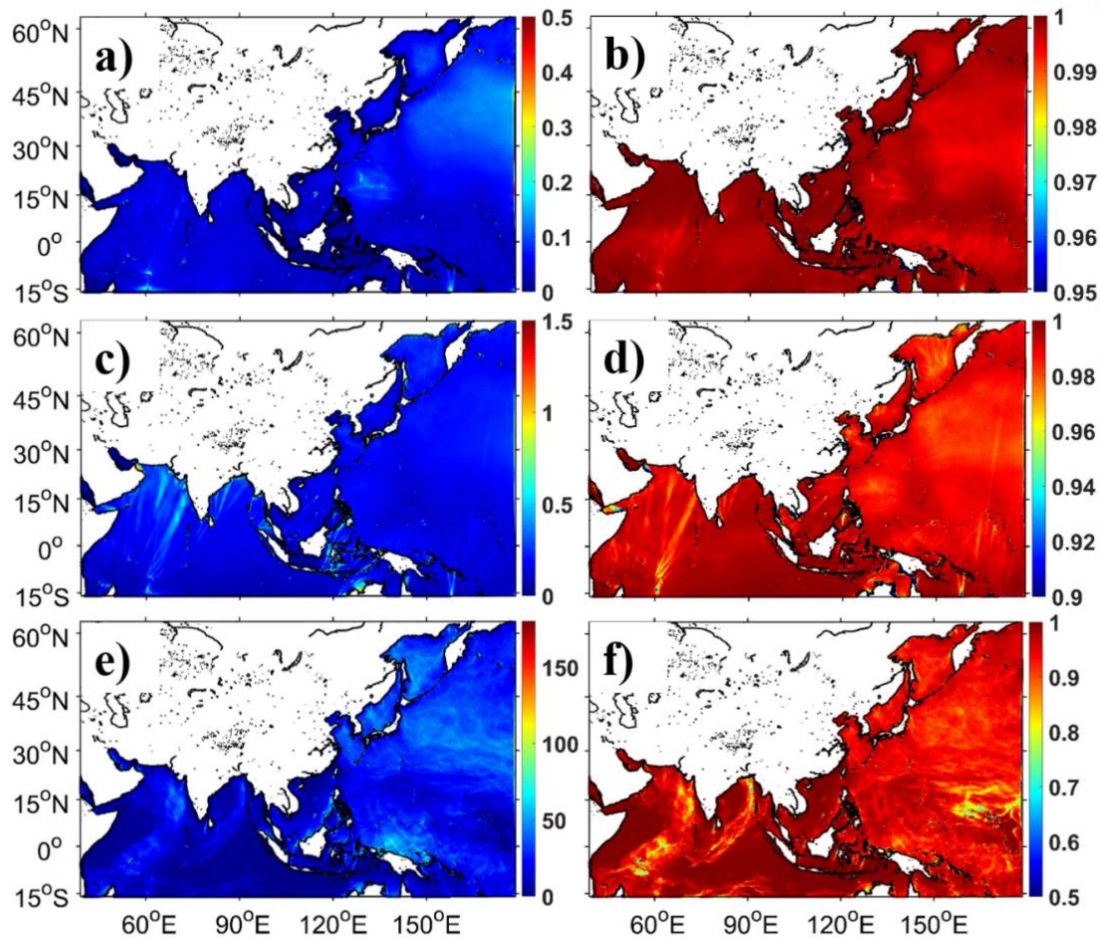

Figure 12: Spatial distributions of RMSDs (a, c, e) and CCs (b, d, f) of SWHs (a, b), MWPs (c, d), and MWDs (e, f) from WS_{multi4}^{utms} in 2018 (unit of panel a/c/e: meter/second/degree). The $WS_{0.125}^{ut}$ in Tab. 1 is considered as a reference to calculate the RMSDs and CCs by linear interpolation.

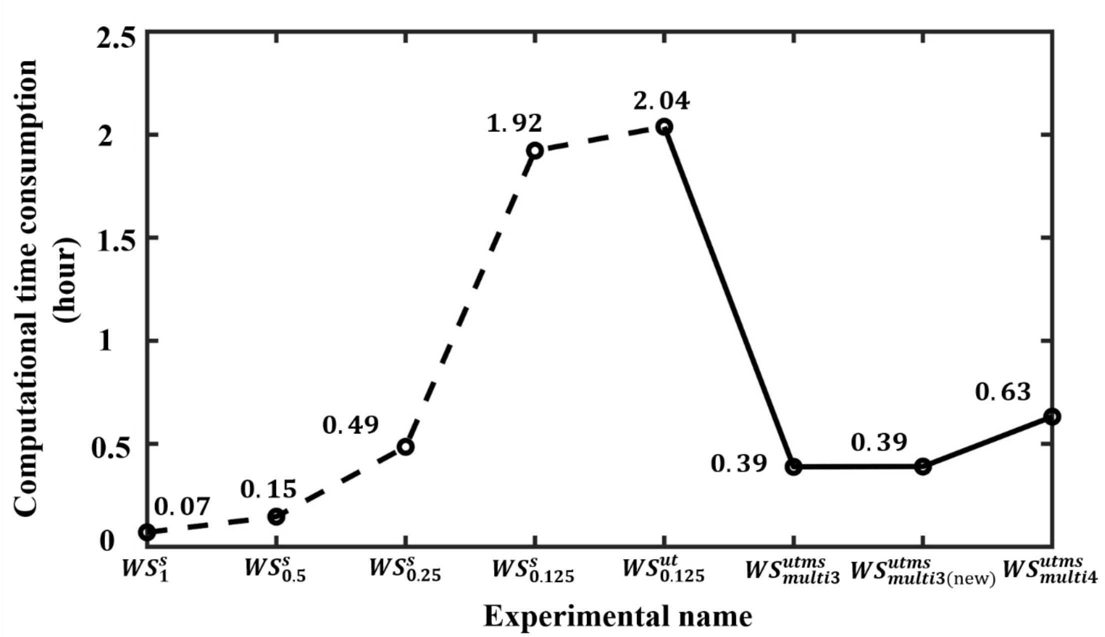

Figure 13: The computational time consumption from wave simulation with unstructured triangular (multiscale) grid systems (solid lines) under the same computational condition. The computational time consumption from Fig. 3 is plotted here with dashed lines for comparison.

Table 1: Design of wave simulation experiments with different grid systems and model resolutions in Asia-Pacific areas.

The name of the experiments	Grid types	Model resolutions	Numbers of water points (or nodes)	The role of experiments
WS_{1}^{s}	Structured grid	1 °lat×1 °lon	6, 454	The performance of wave simulation with different model resolutions
$WS_{0.5}^{s}$	Structured grid	0.5 °lat×0.5 °lon	25, 626	The performance of wave simulation with different model resolutions
$WS_{0.25}^{s}$	Structured grid	0.25 °lat×0.25 °lon	102, 325	The performance of wave simulation with different model resolutions
$WS_{0.125}^{s}$	Structured grid	0.125 °lat×0.125 °lon	408, 511	The performance of wave simulation with different model resolutions
$WS_{0.0625}^{s}$	Structured grid	0.0625 °lat×0.0625 °lon	1, 632, 638	The reference
$WS_{0.125}^{ut}$	Unstructured triangular grid	0.125 ° in whole water areas	521, 911	The reference
WS_{multi3}^{utms}	Unstructured triangular multiscale grid	0.125 °, 0.5 °, and 1 ° in shallow, transitional, and deep water areas	90, 652	The performance of wave simulation in strong wind areas
$WS_{multi3(new)}^{utms}$	Unstructured triangular multiscale grid	0.125 °, 0.5 °, and 1 ° in shallow, transitional, and deep water areas (slight changes in the northern Pacific Ocean area compared with WS_{multi3}^{utms})	91, 472	The performance of wave simulation in strong wind areas
WS_{multi4}^{utms}	Unstructured triangular multiscale grid	0.0625 °, 0.125 °, 0.5 °, and 1 ° in coastal, shallow, transitional, and deep water areas (slight changes around the South China Sea area compared with $WS_{multi3(new)}^{utms}$)	108~~7~~, ~~3~~137	The performance of wave simulation in complex topography areas

Note: to reduce the uncertainty, the maximum global time step, maximum CFL time step for geographic and spectral space, and minimum source-sink term time step in all experiments are the same, which are 900s, 90s, 300s, and 10s, respectively.

Table 2: the information of Chinese oceanic observation stations used in this paper.

Station name	Longitude (°E)	Latitude (°N)	Water depth (m)	Data available in 2018
XMD	120.4	36.0	19.4	Jan. – Dec.
XCS	122.7	39.2	16.7	Jan. – Dec.
NJI	121.1	27.5	16	Jan. – Dec.
BSG	120.3	26.7	10.4	Jan. – Dec.
LHT	121.7	38.9	9.5	Jan. – Mar., May – Dec.
ZLG	115.6	22.7	8.3	May, Jul. – Sep.
DCN	121.9	28.5	5.7	Jan., Feb., May – Dec.
LYG	119.4	34.8	4.7	Jan. – Dec.
DSN	117.5	23.8	1.7	Feb., Mar., May, Jul. – Dec.

Table 3: The performance of WS_{multi3}^{utms} and the reference $WS_{0.125}^{ut}$ both using four propagation schemes in January 2018.

Propagation scheme	SWH		MWP		MWD		Computational time (hour)		
	RMSD (m)	CC	RMSD (s)	CC	RMSD (°)	CC	$WS_{0.125}^{ut}$	WS_{multi3}^{utms}	Improved (%)
CRD-N	0.06	0.991	0.18	0.984	23.72	0.927	2.04	0.39	81%
CRD-PSI	0.08	0.986	0.2	0.979	24.8	0.92	2.11	0.4	81%
CRD-FCT	0.08	0.986	0.21	0.978	25.22	0.915	4.3	0.74	83%
Implicit N	0.07	0.988	0.18	0.982	23.64	0.928	3.84	0.67	83%

Note: simulation results of WS_{multi3}^{utms} are interpolated onto the reference grid to calculate the RMSDs and correlation coefficients (CCs) of SWH, mean wave period (MWP), and mean wave direction (MWD), respectively.

Table 4: The RMSDs and CCs statistics of SWHs, MWPs, and MWDs from WS_{multi4}^{utms} compared with the reference $WS_{0.125}^{ut}$ in 2018.

Boreal Seasons (months)	SWH		MWP		MWD	
	RMSD (m)	CC	RMSD (s)	CC	RMSD (°)	CC
Winter (DJF)	0.09	0.996	0.21	0.993	31.14	0.957
Spring (MAM)	0.07	0.997	0.21	0.994	21.54	0.964
Summer (JJA)	0.06	0.998	0.19	0.995	17.81	0.962
Autumn (SON)	0.08	0.996	0.22	0.993	26.87	0.948
Annual mean	0.08	0.997	0.21	0.994	24.34	0.958